3D Trench-parallel Flow in the Subduction Region and Correlation with Seismic Anisotropy Direction

Tannistha Maiti

Thesis submitted to the faculty of the Virginia Polytechnic Institute and State University in partial fulfillment of the requirements for the degree of

Master of Science
In
Geosciences

Scott D. King, Chair
Robert P. Lowell
Ying Zhou

July 27th, 2012
Blacksburg, VA

Keywords: Subduction, Numerical model, Trench-parallel flow

3D Trench-parallel Flow in the Subduction Region and Correlation with Seismic Anisotropy Direction

Tannistha Maiti

(ABSTRACT)

The motivation of this study is to understand the seismic anisotropy observations from various subduction regions of the world. In subduction zone backarcs both trench-parallel and trench-normal seismic anisotropy, or fast wave polarization direction of shear wave, are observed. In the mantle the general assumption is that seismic anisotropy is caused by Lattice Preferred Orientation (LPO) of olivine minerals and, that the direction of anisotropy is an indicator of the direction of mantle flow. The complex pattern of seismic anisotropy observations suggests that the flow geometry in the vicinity of subduction zones differs at different subduction zones with some subduction zones having trench perpendicular flow, consistent with corner flow in the mantle wedge, while other subduction zones have trench parallel flow, consistent with a mode of flow where material from the mantle wedge flows around the edges of the slab. It should be noted that the direction of LPO orientation can also be modified by the presence or absence of water, pressure, and temperature in the mantle and that it is possible that the difference in anisotropy observations reflects a difference in water content or thermal structure of back arcs. The aim of this study is to test whether the flow geometry of mantle in numerical subduction calculations can influence the direction of seismic anisotropy and, if we parameters that control the pattern of flow can be identified. In this study we explicitly assume that seismic anisotropy occurs only due to plastic and dynamic re-crystallization of mantle mineral forming LPO. To approach the problem two different models are formulated. In one of the models the trench evolves self-consistently, with no prescribed artificial zones of weakness. The self-consistent model has a sticky-air layer at the top of the model domain that mimics a “free-surface”. The other model has the same initial conditions but a trench-migration velocity boundary condition is imposed to the model. The mantle flow pattern for the self-consistent model is consistent with the 2D corner flow model with no flow around the trench and no trench migration. However when the trench-migration velocity boundary condition is imposed, 3D flow around the mantle is observed. The stress field from these simulations are used to calculated instantaneous strain axis directions which correlate with LPO

directions. The LPO orientations are measured from the models showing that the seismic-anisotropy direction is primarily trench-perpendicular for both models. Because the models have different flow patterns, the trench-perpendicular anisotropy alignment that is calculated for both the models is a bit puzzling. It could be that factors such as high temperature and non-linear rheology cause the LPO direction to align trench perpendicular in both the cases. It could also be possible that the 3D vertical flow is not strong enough to cause change in orientation of the LPO direction. From the present study it can be concluded that by looking at the LPO direction nature of mantle flow might not be predicted. This suggests that in addition to flow direction other factors such as the presence of water in mantle wedge, pressure, and high temperature due to viscous coupling modify the seismic anisotropy directions.

DEDICATION

This dissertation is dedicated to my sister Anwita Maiti for all her love in my life.

ACKNOWLEDGEMENTS

I wish to thank my advisor Professor Scott D. King for the continuous guidance and support he provided me during my graduate studies at Virginia Tech. His patience and expertise has helped me shape from a naïve Geoscientist to a Geoscience researcher. The skill sets that I learned will be greatly useful in my future career.

I would like to express my gratitude to my committee members; Professor Robert P. Lowell and Professor Ying Zhou for their constructive and critical suggestions that helped me improve my work.

My fellow research group members never failed to support me in my endeavors. I would like to thank Ms. Pavithra Sekhar and Ms. Karina Cheung for their generous advice and rapport. I especially thank Ms. Connie Lowe, you are awesome.

I thank my friends Ms. Sharmistha Mitra, Ms. Manjushree Palit, Dr. Lakshmi Dharmarajan, Dr. Sanghamitra Sen and Ms. Mohona Sarkar and Mr. Puranjoy Bhattacharjee and all my friends at Virginia Tech.

Finally, I am most grateful to my parents, Mrs. Mita Maiti and Dr. Biswajit Maiti and my dear sister Ms. Anwita Maiti for their encouragement and endless love over the years.

TABLE OF CONTENTS

LIST OF FIGURES

CHAPTER 1: INTRODUCTION

1.1 Shear Wave Splitting and Observations

The rocks in the Earth's interior, especially in the upper mantle, show some degree of seismic anisotropy. In a seismically anisotropic medium, the velocity of the seismic wave depends on the direction the wave is traveling. Most minerals are anisotropic because of their crystal structure (Karato, 2008). The difference in seismic wave speed with direction causes the wave to separate and this is called the shear-wave splitting. Figure 1.1 shows the relation between splitting pattern and delay time in an isotropic and anisotropic medium (Savage et. al, 1999). Seismic anisotropy is generally documented by measuring the fast component of shear wave and the time delay between the two shear waves (Savage et al., 1999).

The seismic anisotropy in Earth's interior can be inferred from various seismologic observations (Karato, 2007; Long and Becker, 2010). Seismic anisotropy in the upper mantle has been inferred in the upper mantle based on Pn velocities (Hess, 1964; Shearer and Orcutt, 1986), the polarization of long period surface waves (Nataf et al., 1984; Ismail and Mainprice, 1998), from analysis of P travel time residues for the asthenosphere (Bokelmann, 2002) and deep mantle (Boschi and Dziewonski, 2000). Receiver functions also gives information about anisotropic contrast in the upper mantle and crust (Levin and Park, 1998). Analysis of splitting and birefringence of shear wave is a common method to study anisotropy (Long and Silver, 2009). The shear wave splitting method is the most efficient technique to measure anisotropy because it is unaffected by isotropic wave speed heterogeneity (Long and Becker, 2010).

Mantle seismic anisotropy can be related to strain and stress field, the temperature gradient field, and can be used as a tool to understand the dynamic process of Earth also including the flow geometry of the mantle (Karato, 2007). One of the leading hypothesis for the cause of seismic anisotropy in the upper mantle is the lattice preferred orientation (LPO) of olivine the most dominant mineral in the upper mantle (Karato et al., 2008). Lattice preferred orientation results from the non-random distribution of the crystallographic axis in a rock and reflects the history of how rock was deformed or is being deformed in a stress field (Ribe, 1989). McKenzie (1979) and Ribe (1992) have studied the properties of finite deformation in convective mantle flow and have established a connection between finite strain ellipsoid of deformation and LPO formation. While the relationship between strain and lattice preferred orientation is complicated, the maximum strain is expected to align parallel to asthenospheric flow for large strain (Ribe, 1989; Wenk et al., 1989). According to Jung and Karato (2001) in A-type olivine the a-axis of the crystal always aligns to the maximum shear stress direction. While in B-type olivine the b-axis of the crystal always aligns to the maximum shear stress direction. Difference in water and temperature conditions control whether A-type or B-type olivine will occur. If the seismic velocity is known then the elastic constants can be calculated and the mantle flow field can be predicted (Long et al., 2009).

In a subduction region plate and slab motions cause shearing in the mantle that result in lattice-preferred orientation of mantle minerals (Conrad et al., 2007). The mantle flow pattern can be coordinated with the a-axis and the finite strain ellipsoid orientation in LPO's of olivine. The DRex model developed by Kaminski and Ribe (2002) and Kaminski et al. (2004) calculates the LPO orientations from a given mantle field. In this

study, correlation will be made between the predicted mantle flow field of a 3D subduction model, and the orientations of the LPO.

Shear-wave splitting patterns are observed in almost every subduction region of the world. As discussed above, these splitting observations are thought to represent the orientation of the flow of mantle materials above and below the subducting plate (Long and Silver, 2008; Wolfe and Solomon, 1998; Savage and Sheehan, 2000). In subduction region both trench parallel and trench normal splitting patterns are observed. Trench parallel patterns have been inferred from beneath the Ryukyu arc by Long and van der Hilst (2005, 2006), and Russo and Silver (1994) beneath Nazca plate. Fischer et. al. (1998) studied the fast directions of the S and SKS beneath the Izu- Bonin and Tonga arc which are parallel to sub-parallel beneath the trench. Fischer et al. (2000) measured trench parallel polarized shear wave direction in the back arc of Tonga subduction region. Levin et al. (2004) observed trench parallel fast polarization direction in the Kamchatka subduction region. Trench-normal fast polarization was observed by Su and Park, (1994) in the back-arc of the Kuriles and in Pacific Northwest by Schutt and Humphreys (2001) in North America. Fouch and Fischer (1996), Long and van der Hilst (2005), and Fouch et al. (2002) studied Honshu and Ryukyu. Their observations revealed that the fast directions of olivine a-axis rotate from trench-parallel near the trench to trench-orthogonal into the back-arc. Lassak et al. (2006) combined various anisotropy measurements both trench parallel and trench–normal from different subduction regions of the world and compiled those measurements as shown in Figure 1.2. They pointed out that there are discrepancies in splitting directions for different subduction regions which they approached by using lattice-preferred orientation development in steady-state two-

dimensional mantle flow models. They used both hydrated and anhydrous mantle wedge conditions and evaluated shear wave splitting observations in the subduction region around Pacific Rim.

The seismic anisotropy measurements from various subduction regions were compiled by Long and Silver (2008) to present an integrated 3D mantle flow model with trench parallel and trench- normal mantle flow (Figure 1.4). They compiled shear wave splitting behavior from 13 subduction regions of the world. They also combined the average splitting parameters to overriding plate velocity, trench migration rate, stress state of the overriding plate, subducting plate age, convergence rate, slab depth beneath volcanoes, and slab dip. The sub-slab mantle where the stresses are low, water content is low, and relatively high temperature, should have a flow that is trench-parallel. They also observed that subduction systems with stationary trenches are mostly isotropic but for migrating trenches splitting "delay time" increases with migration velocity. There experiments also suggested that there is good coherence between trench migration velocity and delay time. The velocity of convergence and back-arc deformation rate for various subduction zones have been complied in Figure 1.3. The data is taken from Cruciani et al. (2005). The subduction zones that lie above the line should be typically showing trench-perpendicular anisotropy direction and the region below the line show trench-perpendicular anisotropy behavior. It is observed from the plot that the Tonga-Kermadac subduction region show trench-parallel anisotropy behavior. Based on the results of Fischer et al., (2000), LPO develop trench-parallel everywhere in the mantle to a depth of 410 km in the back-are region and it is associated with high stress conditions. The plot also shows that the Mariana-Japan subduction zones has trench-perpendicular

conditions. To support such observations Nakajima and Hasegawa (2004) argued that back-arc region contains less water and hence it has trench-perpendicular flow conditions.

Based on their observations of trench migration velocity and delay time, Long and Silver (2008) suggested that sub-slab mantle anisotropy is controlled by 3D return flow. 3D return flow occurs due to trench migration, while, 2D corner flow field in the mantle wedge occurs due to viscous coupling between the downgoing slab and the overlying wedge. The 3D perspective subduction model proposed by Long and Silver (2008) has two dominant mantle flow fields (Figure 1.4): a 2D corner flow that controls the coupling between the subducting slab and the overlying wedge (Nakajima and Hasegawa, 2004; Kneller, et. al., 2005), and a 3D flow field where mantle flows around the slab due to migration of subduction system known as the trench rollback. In a 3D return flow the slab rolls back from the arc (i.e., trench migrates in the direction of the subducting plate) and material from behind/beneath the slab flows around the edges of the slab, conserving mass. This flow around the slab is parallel to the trench except near the slab edge and is perpendicular to the 2D wedge corner flow. These flow fields were also predicted by Lassak et al. (2006) based their simple 2D models.

The phenomenon of trench parallel flow has been observed in laboratory tank models by Funiciello et al. (2003a and 2003b), Kincaid and Griffiths (2003), and Buttles and Olson (1998). Numerical experiments by Piromallo et al. (2006), Schellart et al. (2007), and Stegman et al. (2006) also observed trench rollback. Earlier 2D numerical subduction modelers have imposed trench roll-back velocities and observed the simulations having retrograde motions (Christensen, 2001; Christensen, 1996; Conrad

and Lithgow-Bertelloni, 2007). Christensen (2001) observed that the trench roll-back was pronounced when the slab flattens at the interface between the upper and the lower mantle. Di Giuseppe et al. (2008) worked with subduction model to investigate the factors that might be dominantly controlling the trench migration. They used both two and three dimensional numerical modeling. Their observations lead to the hypothesis that stiffer slabs causes the trench to advance, whereas more flexible slabs causes the trench to retreat.

Evidence of trench rollback has also been observed from geological data in the backarc of subduction regions. Episodic deformation is observed because of trench migration (Taylor and Karner, 1983; Khazaradze and Klotz, 2003). In accordance with Tao and O'Connell (1993) when slab bends during subduction deformation occurs indicating zones of weakness. Bevis et al. (1995) measured the fast extension of Lau basin and back-arc extension of the Tonga subduction zone indicating trench migration velocities of 16 cm/yr from GPS data. Kato et al. (1998) saw roll back effect and back-arc spreading of 4.4 and 5 cm/yr respectively form the Ryukyu and the Mariana subduction zone. Trench migration rate at the Andrean trench is about 1cm/yr (Sella et al., 2002). Trench migration rates have also been documented at the Calabrian trench and Helentric Trench (Faccenna et al., 2003; Heidbach and Ben-Avraham, 2007; McClusky et al., 2000). It is assumed that the lithospheric plates are moving with respect to fixed reference frame that is usually constrained by hotspots. NUVEL -1 is a plate velocity model developed by DeMets et al. (1990) to determined plate velocity with respect to hotspot data. With this theory subduction regions will also be moving with respect to the fixed reference frame. Heuret and Lallemand (2005) suggested that plate motion, trench

motion, back-arc deformation rate, upper plate strain regime and slab age in oceanic subduction zones are important parameters for trench migration. They also proposed that back-arc extends when the plate retreats and contracts when the plate advances.

1.2 Subduction Phenomenon

The lifetime of a subduction process is about 200 Ma (Rowland and Davies, 1999) for the plate to completely subduct beneath the overriding plate. It is not possible to monitor geophysical parameters for such a time length. Numerical and laboratory subduction models parameters are taken based on present day seismic tomography images, geoids, topography, GPS data and shear-wave splitting data (King, 2007). The physics of subduction is complex and involves a large number of forces. The main driving force is buoyancy. The buoyancy difference between the slab and mantle drives subduction. Due to buoyancy the oceanic lithosphere sinks into the lower mantle at a dip angle of nearly 90˚. Two factors that can also contribute to subduction are the lateral density difference between the continental crust and the adjacent oceanic crust and a chemical density contrast between continental and oceanic lithospheric mantle. These have been investigated by Nikolaeva et al. (2011) by numerical modeling. The main forces that are associated with subduction are the ridge push, slab pull and trench suction (Forsyth and Uyeda, 1975). Ridge pull is a horizontal pressure gradient due to the cooling of the subducting plate (Lister, 1975) whereas slab pull is a plate boundary force that depends on the slab length, slab thickness and angle of subduction (Vlaar and Wortel, 1976). Trench suction forces are associated with the overriding plate (Wilson, 1993). The evolution of a subducting slab and the deformation of slab with time are also very

complex. The different stress condition of the slab creates region of extension and compression. From analysis of global Centroid Moment Tensor catalog Bailey et al. (2012) divided a subduction slab into intermidate –extensional, intermediate extensional deep compressional, and intermediate to deep compressional categories. Because so many forces are associated, subduction models have to be simplified. For many years researchers have done laboratory and numerical modeling by varying rheology and plate boundary conditions. Most of the rheologies used have been simple and dependent on temperature, pressure and simple velocity boundary conditions (Funiciello et al., 2003a; Funiciello et al., 2003b; Kincaid and Griffiths, 2003). Kinematic plate conditions are often applied to understand subduction in the view of global scale.

1.3 Subduction Models

Subduction models are studied at both global and region scales. In a global model first –order observations like force-balanced plate motion, the geoid and tomographically mapped deep slab anomalies are examined (Becker and Faccenna, 2009). In a regional model on the other hand, an isolated slab is considered that enters into the mantle and the sidewall boundary conditions are no-slip or periodic (Zhong and Gurnis 1992; Ita and King, 1998; Chen and King, 1998; Han and Gurnis, 1999; Zhong and Gurnis 1995; Enns et al. 2005; Stegman et al., 2006; Billen and Hirth, 2007). The dynamics of subduction are controlled by the rheology of the slab and mantle which depends on temperature, composition, grain size, water content and melt fraction (Billen, 2008).

In a mantle convection problem it is important to constrain the motion of lithosphere, the kinematics of the lithosphere are necessary to include as a boundary

condition for deep mantle flow (Hager and O'Connell, 1979). For example by uniform plate velocity in a particular direction, the symmetrical spreading at the ridges and asymmetrical convergence at trench, rate of subduction and trench migration (e.g. Gurnis and Davies, 1986; Billen, 2008). However for solving the subduction problem it should be kept in mind that the kinematic conditions do not create self-consistent dynamic evolution, of the slab and may end up controlling the flow surrounding the slab, thus prescribing the very flow that is the focus of this study. As observed by Enns et al., (2005), periodic and reflecting velocity boundary conditions have a totally different effect on the evolution of slab in a model that is otherwise identical.

In recent years researchers have focused on using dynamically self-consistent numerical models (Gurnis and Hager, 1988; Ita and King, 1994; Zhong and Gurnis, 1995;King and Ita, 1998; Funiciello et al., 2003b; Enns et al., 2005; Stegman et al., 2006; Lee and King 2011) and laboratory models (Funiciello et al., 2003a; Bellahsen et al., 2005; Faccenna et al., 2007). The term 'self-consistent' referrs to subduction driven due to buoyancy forces because of the temperature contrast between the slab and upper mantle without including prescribed zones of weakness. Both numerical and laboratory experiments show that the slab strength controls the subduction velocity and its partitioning between trench and plate motion (Di Giuseppe et al., 2008). However, to model a self-consistent subduction region the major challenge is to apply a method so as to decouple the subducting slab from the surface of the overriding plate. Early models were based on weakened mantle region near the trench while others neglected the overriding plate (Schmeling and Jacoby, 1981; King and Hager, 1990; Becker et al., 1999; Funiciello et al., 2004, Funiciello et al., 2006; Kincaid and Olson, 1987; Martinod

et al., 2005; Schellart, 2004; 2005; Stegman et al., 2006). Buttles and Olson (1998) and Kincaid and Griffiths (2003) in 3D laboratory model included lateral slab hence kinematically explaining the trench movement. Whereas Faccenna et al. (2001), Funiciello et al. (2004); Funiciello et al. (2003a); Funiciello et al. (2003b); Funiciello et al. (2006) and Schellart (2004) and (2005) and Schellart et al. (2007) have used a purely dynamically self-consistently model. 3D numerical subduction models have been studied e.g. by Stegman et al. (2006) and Schellart et al. (2007). In these models the decoupling zones evolve self-consistently. In the recent benchmark paper by Schmeling et al. (2008) the modeling of the decoupling zones are archived by a low-viscosity, zero density, top layer which has been termed a "sticky-air" layer. Relating this to Earth, the sticky-air layer can be compared to a layer of low density sediment over the plates.

1.4 Computing Subduction Models

The mantle flow is complicated process including both regions of linear and non-linear rheology (Zhong et al., 1998; Moresi and Solomatov, 1998). The deformation processes that occur at plate margins also play an important role (King and Hager, 1990; Zhong and Gurnis, 1996) and this adds to the complexity. The simulation of subduction models are both regional and global take a lot of computer time. High-performance parallel computing facilities and sophisticated modeling software for mantle convection are used to model 3D spherical shell geometry (Moresi et al., 2000, Zhong et al., 2008). Parallel computing is now widely used to do mantle convection research (Gurnis et. al, 1988, Tackley et al., 1994). Parallel computing was used as early as 1994 by Tackley et al. (1994) for a finite volume code and a spectral convection code (Glatzmaier, 1988)

using parallel processing super computer Intel Delta. Today improvements in inter-processor communication speed and message passing software mean that parallel computing has proved very effective in large simulations including many of the recent papers. CitcomS, a finite element code is designed to solve compressible thermo-chemical convection problems and runs in parallel processing computers, including both shared and distributed platforms (Zhong et al., 2000; Tan et al., 2006). Parallel computing in CitcomS is enabled by MPI for interprocessor communications (Zhong et al. 1998, Moresi et al., 2000). CitcomS can use a nonorthogonal mesh that consists of equal or unequal mesh elements. CitcomS is ideal for subduction studies because it can use preexisting fault directly incorporated in the mantle, or non-linear power law rheology. The faults are considered as internal lines and planes along which the normal velocity is continuous. Flow on either side of the fault is coupled through frictional stresses. CitcomS includes both multigrid and preconditioned conjugate gradient solver at the inner level iterations.

Various other mantle convection code for both 2D and 3D formulations use parallelized version. FEMS-2D written by Frehner and Schmalholz, (2006) and Schmalholz (2006) is a finite element code for simulating slow incompressible flows in two dimensions. The higher order elements for the velocities are used in combination with linear elements for the pressure and the approach is called mixed velocity–pressure formulation to incompressible flow. The viscous and the viscoelastic code by (Gerya and Yuen, 2003; 2007) called I2VIS and I2ELVIS respectively are based on a combination of finite differences (pressure–velocity formulation on fully staggered grid) with marker-in-cell technique. Markers carry information on composition such as density, viscosity and

shear modulus,and stresses in viscoelastic case. Viscosity, density and stresses are interpolated from markers to nodes by using bilinear distance. The code FDCON by Schmeling and Marquart (1991) is a finite difference and was rewritten as biharmonic equation in terms of the stream function and variable viscosity. The FD formulation of the biharmonic equation results in a symmetric system of linear equations, which is directly solved by Cholesky decomposition. The code ConMan (King et al., 1990) is a vectorized finite element code that is based on 2D incompressible, thermal convection with infinite Prandlt number.

1.5 Lattice Preferred Orientation of Olivine and Upper Mantle Rheology

In Earth's upper mantle the dominant mineral is olivine with a volume fraction of 40-60% in the upper mantle. Because olivine is the weakest upper mantle mineral it controls the rheology of the mantle (Karato and Wu, 1993). The creep properties of olivine dependence on temperature, pressure, and grain size (Weertman, 1970; Goetze and Evans, 1979; Chopra and Paterson, 1984; Karato et al., 1986; Bai et al., 1991; Hirth and Kohlstedt, 1995; Mei and Kohlstedt, 2000; Karato and Jung, 2003). Lattice preferred orientation of olivine in polycrystalline aggregates is observed because of the alignment of slip plane direction to the direction of shear plane (Ribe and Yu, 1991; Wenk and Christie, 1991). The two most dominant deformation mechanisms in the upper mantle are diffusion and dislocation creep. Karato and Wu (1993) pointed out that the transition between the diffusion and dislocation creep occurs in Earth's upper mantle. In the presence of dislocation creep there is dynamic recrystallization by subgrain rotation and grain boundary migration (Zhang et al., 2000; Lee et al., 2002). Nicolas et al. (1973),

Mainprice and Nicolas (1989), and Zhang and Karato (1995) studied models based on laboratory creep laws for dry olivine and showed that olivine is compatible with average radial viscosity profiles, toroidal and poloidal type of velocity and also partitioning of fabric into anisotropy formation under dislocation creep in the upper mantle. Kaminski and Ribe (2002) developed a model for plastic deformation and dynamic recrystalization that determines LPO orientation and the model has been used in the present study.

The upper mantle exhibits power-law creep behavior (Ranalli, 1995). Hence the upper mantle is modeled using a simple Arrhenius law (Karato and Wu, 1993) and laboratory values for activation energy, activation volume and stress exponents of olivine are used. Viscosity is both temperature and shear stress dependent. Temperature and yield stress dependent rheology has earlier been used by Lee and King (2009), Tackley (1997), Tackley et al. (2000) in computation of dynamics of subduction. Billen and Hirth (2007) have used stress dependent rheology and the values of deformation are obtained from laboratory measurements. They found that slabs are stiff due to strong temperature dependence on viscosity.

Upper mantle anisotropy is likely formed by progressive deformation of olivine under dislocation creep (Nicolas and Christensen, 1987). The inclusion of power law viscosity, which is based on the dislocation creep, is particularly important to study seismic anisotropy. Dislocation creep, however, takes place only when deviatoric stress exceeds some critical value and below this value diffusion creep predominates. The critical stress is known to depend on temperature, pressure, grain size, and water content (Karato, 2008). Thus to study mantle flow and seismic anisotropy it is essential to work with composite rheology, which deals with both creep mechanisms.

Also it has been shown that subducting slabs are more viscous than the surrounding mantle (King and Hager, 1994). Geoid models (Moresi and Gurnis 1996 and Billen et al. 2003) show that the subducting slab might be 100 times more viscous than the surrounding mantle. Earthquake depth distribution and orientation of stresses in slabs are also consistent with an increase in viscosity between slab and mantle(Vassiliou et al., 1984; Tao and O'Connell, 1993).

Finally, in this thesis I will try to address whether slab rollback is sufficient to create the 3D flow as is show in Figure 1.4, are whether trench parallel flow is associated with rollback and under what circumstances are the subduction systems isotropic and anisotropic. The numerical model will be addressed by using free–subduction model or self-consistent subduction as discussed earlier. Considering the fact that dislocation creep contributes to anisotropy; how the introduction of different creep modifes the flow pattern will also be investigated. The model will be used with a viscosity difference between the upper and lower mantle so as to generate flow, consistent with the geoid.

The next part of the problem is to use mantle flow model to identify of LPO development and shear wave splitting (Fischer et al., 2000; Fouch et al., 2000; Hall et al. 2000; Kaminski and Ribe, 2001; Lassak et al., 2006; Long et al., 2007). The LPO will be mapped in terms of fast axis orientation of mantle mineral mostly olivine and a bit of enstatite (Kaminski and Ribe, 2001, Conrad et al., 2007). Because shear wave splitting observation have reveled both trench parallel and trench perpendicular flow in subduction regions, 3D flow models and LPO analysis will be main tools. Laboratory experiments by Funiciello et al. (2003 and 2006) have already found that trench rollback is common and, the numerical model will be tested using the tank experiment parameters. Also

experiments will be done by imposing trench migration velocity and to observe the flow pattern. The model domain will be a regional model taken as part of a 3D spherical shell as described by CitcomS which will be a real Earth reproduction. We will use simple stress free boundary conditions.

References

Bai, Q., S. J. Mackwell, and D. L. Kohlstedt (1991), High-Temperature creep of olivine single-crystals: Mechanical results for buffered samples, *J. Geophys. Res.-Solid Earth and Planets, 96(B2)*, 2441-2463.

Bailey, I. W., L. A. Alpert, T. W. Becker, and M. S. Miller (2012), Co-seismic deformation of deep slabs based on summed CMT data, *J. Geophys. Res.-Solid Earth*, *117*, B04404, doi:10.1029/2011JB008943.

Becker, T. W. (2006), On the effect of temperature and strain-rate dependent viscosity on global mantle flow, net rotation, and plate-driving forces, *Geophys. J. Int.*, *167*(2), 943-957.

Becker, T.W., C. Faccenna (2009), A review of the role of subduction dynamics for regional and global plate motions, Lallemand, S., Funiciello, F. (eds.) *Subduction Zone Geodynamics*, doi: 10.1007/978-3-540-87974-9, Springer-Verlag Berlin HeidelbergSpringer, 3–34

Becker, T. W., C. Faccenna, R. J. O'Connell, and D. Giardini (1999), The development of slabs in the upper mantle: Insights from numerical and laboratory experiments, *J. Geophys. Res.-Solid Earth*, *104*(B7), 15,207-15,226.

Bellahsen, N., C. Faccenna, and F. Funiciello (2005), Dynamics of subduction and plate

motion in laboratory experiments: Insights into the "plate tectonics" behavior of the Earth, *J. Geophys. Res.-Solid Earth*, *110*, B01401, doi: 10.1029/2004JB002999

Ben Ismail, W., and D. Mainprice (1998), An olivine fabric database: An overview of upper mantle fabrics and seismic anisotropy, *Tectonophysics*, *296*(1-2), 145-157.

Bevis, M., et al. (1995), Geodetic observations of very rapid convergence and back-arc extension at the Tonga Arc, *Nature*, *374*(6519), 249-251.

Bijwaard, H., W. Spakman, and E. R. Engdahl (1998), Closing the gap between regional and global travel time tomography, *J. Geophys. Res.-Solid Earth*, *103*(B12), 30,055-30,078.

Billen, M. I. (2008), Modeling the dynamics of subducting slabs, *Annual Review of Earth and Planetary Sciences*, *36*, 325–356.

Billen, M. I., and M. Gurnis (2003), Comparison of dynamic flow models for the Central Aleutian and Tonga-Kermadec subduction zones, *Geochem. Geophys. Geosyst.*, *4*(4), 1035, doi:10.1029/2001GC000295.

Billen, M. I., and G. Hirth (2007), Rheologic controls on slab dynamics, *Geochem. Geophys.Geosyst.*, *8*, Q08012, doi: 10.1029/2007GC001597

Billen, M. I., M. Gurnis, and M. Simons (2003), Multiscale dynamics of the Tonga-Kermadec subduction zone, *Geophys. J. Int.*, *153*(2), 359-388.

Bokelmann, G. H. R. (2002), Convection-driven motion of the north American craton: Evidence from P-wave anisotropy, *Geophys. J. Int.*, *148*(2), 278-287.

Boschi, L., and A. M. Dziewonski (2000), Whole Earth tomography from delay times of

P, PcP, and PKP phases: Lateral heterogeneities in the outer core or radial anisotropy in the mantle?, *J. Geophys. Res.-Solid Earth, 105*(B6), 13,675-13,696.

Buttles, J., and P. Olson (1998), A laboratory model of subduction zone anisotropy, *Earth Planet. Sci. Lett., 164*(1-2), 245-262.

Chapple, W. M., and T. E. Tullis (1977), Evaluation of forces that drive plates, *J. Geophys. Res., 82*(14), 1967-1984.

Chopra, P. N., and M. S. Paterson (1984), The role of water in the deformation of Dunite, *J. Geophys. Res., 89*(NB9), 7861-7876.

Christensen, U. (2001), Geodynamic models of deep subduction, *Phys. Earth Planet. Inter., 127*(1-4), 25-34.

Christensen, U. R. (1996), The influence of trench migration on slab penetration into the lower mantle, *Earth Planet. Sci. Lett., 140*(1-4), 27-39.

Conrad, C. P., and C. Lithgow-Bertelloni (2007), Faster seafloor spreading and lithosphere production during the mid-Cenozoic, *Geology, 35*(1), 29-32.

Conrad, C. P., M. D. Behn, and P. G. Silver (2007), Global mantle flow and the development of seismic anisotropy: Differences between the oceanic and continental upper mantle, *J. Geophys. Res.-Solid Earth, 112* B07317. doi:10.1029/2006JB004608

Cruciani, C., E. Carminati, and C. Doglioni (2005), Slab dip vs. lithosphere age: No direct function, *Earth Planet. Sci. Lett., 238*(3-4), 298-310.

Demets, C., R. G. Gordon, D. F. Argus, and S. Stein (1990), Current plate motions, *Geophys. J. Int., 101*(2), 425-478.

Di Giuseppe, E., J. van Hunen, F. Funiciello, C. Faccenna, and D. Giardini (2008), Slab

stiffness control of trench motion: Insights from numerical models, *Geochem. Geophys. Geosyst., 9*, Q02014. doi:10.1029/2007GC001776.

Di Giuseppe, E., C. Faccenna, F. Funiciello, J. van Hunen, and D. Giardini (2009), On the relation between trench migration, seafloor age, and the strength of the subducting lithosphere, *Lithosphere*, *1*(2), 121-128.

Enns, A., T. W. Becker, and H. Schmeling (2005), The dynamics of subduction and trench migration for viscosity stratification, *Geophys. J. Int.*, *160*(2), 761-775.

Faccenna, C., L. Jolivet, C. Piromallo, and A. Morelli (2003), Subduction and the depth of convection in the Mediterranean mantle, *J. Geophys. Res.-Solid Earth*, *108*(B2), 2099, doi:10.1029/2001JB001690.

Faccenna, C., T. W. Becker, F. P. Lucente, L. Jolivet, and F. Rossetti (2001), History of subduction and back-arc extension in the Central Mediterranean, *Geophys. J. Int.*, *145*(3), 809-820.

Faccenna, C., A. Heuret, F. Funiciello, S. Lallemand, and T. W. Becker (2007), Predicting trenchand plate motion from the dynamics of a strong slab, *Earth Planet. Sci. Lett.*, *257*(1-2), 29-36.

Fischer, K. M., M. J. Fouch, D. A. Wiens, and M. S. Boettcher (1998), Anisotropy and flow in Pacific subduction zone back-arcs, *Pure Appl. Geophys.*, *151*(2-4), 463-475.

Fischer, K. M., E. M. Parmentier, A. R. Stine, and E. R. Wolf (2000), Modeling anisotropy and plate-driven flow in the Tonga subduction zone back arc, *J. Geophys. Res.-Solid Earth*, *105*(B7), 16,181-16,191.

Flanagan, M. P., and D. A. Wiens (1994), Radial upper-mantle attenuation structure of

inactive back-arc basins from differential shear-wave measurements, *J. Geophys. Res.-Solid Earth*, *99*(B8), 15,469-15,485.

Forsyth, D., and S. Uyeda (1975), Relative importance of driving forces of plate motion, *Geophysical Journal of the Royal Astronomical Society*, *43*(1), 163-200.

Fouch, M. J., and K. M. Fischer (1996), Mantle anisotropy beneath northwest Pacific subduction zones, *J. Geophys. Res.-Solid Earth*, *101*(B7), 15,987-16,002.

Fouch, M. J., and K. M. Fischer (1998), Shear wave anisotropy in the Mariana subduction zone, *Geophys. Res. Lett.*, *25*(8), 1221-1224.

Fouch, M. J., K. M. Fischer, and M. E. Wysession (2002), Lowermost mantle anisotropy beneath the Pacific: Imaging the source of the Hawaiian plume, *Earth Planet. Sci. Lett.*, *195*(3-4), 299-300.

Frehner, M., and S. M. Schmalholz (2006), Numerical simulations of parasitic folding in multilayers, *J. Struct. Geol.*, *28*(9), 1647-1657.

Funiciello, F., C. Faccenna, and D. Giardini (2004), Role of lateral mantle flow in the evolution of subduction systems: Insights from laboratory experiments, *Geophys. J. Int.*, *157*(3), 1393-1406.

Funiciello, F., C. Faccenna, D. Giardini, and K. Regenauer-Lieb (2003a), Dynamics of retreating slabs: 2. Insights from three-dimensional laboratory experiments, *J. Geophys. Res.-Solid Earth*, *108*(B4), 2207, doi:10.1029/2001JB000896

Funiciello, F., G. Morra, K. Regenauer-Lieb, and D. Giardini (2003b), Dynamics of retreating slabs: 1. Insights from two-dimensional numerical experiments, *J. Geophys. Res.-Solid Earth*, *108*(B4), 2206, doi:10.1029/2001JB000898.

Funiciello, F., M. Moroni, C. Piromallo, C. Faccenna, A. Cenedese, and H. A. Bui

(2006), Mapping mantle flow during retreating subduction: Laboratory models analyzed by feature tracking, *J. Geophys. Res.-Solid Earth*, *111*(B3), B03402, doi:10.1029/2005JB003792

Gerya, T. V., and D. A. Yuen (2003), Characteristics-based marker-in-cell method with conservative finite-differences schemes for modeling geological flows with strongly variable transport properties, *Phys. Earth Planet. Inter.*, *140*(4), 293-318.

Gerya, T. V., and D. A. Yuen (2007), Robust characteristics method for modelling multiphase visco-elasto-plastic thermo-mechanical problems, *Phys. Earth Planet. Inter.*, *163*(1-4), 83-105.

Glatzmaier, G. A. (1988), Numerical simulations of mantle convection - time-dependent, 3-dimensional, compressible, spherical-shell, *Geophys. Astrophys. Fluid Dyn.*, *43*(2), 223-264.

Goetze, C., and B. Evans (1979), Stress and temperature in the bending lithosphere as constrained by experimental rock mechanics, *Geophysical Journal of the Royal Astronomical Society*, *59*(3), 463-478.

Gurnis, M., and G. F. Davies (1986), Numerical study of high Rayleigh number convection in a medium with depth-dependent viscosity, *Geophysical Journal of the Royal Astronomical Society*, *85*(3), 523-541.

Gurnis, M., and B. H. Hager (1988), Controls of the structure of subducted slabs, *Nature*, *335*(6188), 317-321.

Hager, B. H., and R. J. O'Connell (1979), Kinematic models of large-scale flow in the Earth's mantle, *J. Geophys. Res.*, *84*(NB3), 1031-1048.

Hayes, G. P., D. J. Wald, and R. L. Johnson (2012), Slab1.0: A three-dimensional model

of global subduction zone geometries, *J. Geophys. Res.-Solid Earth*, *117*, B01302, doi:10.1029/2011JB008524

Heidbach, O., and Z. Ben-Avraham (2007), Stress evolution and seismic hazard of the Dead Sea Fault System, *Earth Planet. Sci. Lett.*, *257*(1-2), 299-312.

Heuret, A., and S. Lallemand (2005), Plate motions, slab dynamics and back-arc deformation, *Phys. Earth Planet. Inter.*, *149*(1-2), 31-51.

Hess,H.H.,(1964), Seismic Anisotropy of the uppermost mantle under oceans, *Nature, 203* (4945), 629-631.

Hirth, G., and D. L. Kohlstedt (1995), Experimental constraints on the dynamics of the partially molten upper-mantle: Deformation in the dislocation creep regime, *J. Geophys. Res.-Solid Earth*, *100*(B8), 15,441-15,449.

Jung, H., and S. I. Karato (2001), Effects of water on dynamically recrystallized grain-size of olivine, *J. Struct. Geol.*, *23*(9), 1337-1344.

Kaminski, E., and N. M. Ribe (2002), Timescales for the evolution of seismic anisotropy In mantle flow, *Geochem. Geophys. Geosyst.*, *3(8),* 1050, doi:10.1029/2001GC000222.

Kaminski, E., N. M. Ribe, and J. T. Browaeys (2004), D-Rex, a program for calculation of seismic anisotropy due to crystal lattice preferred orientation in the convective upper mantle, *Geophys. J. Int.*, *158*(2), 744-752.

Fischer, K. M., E. M. Parmentier, A. R. Stine, and E. R. Wolf (2000), Modeling anisotropy and plate-driven flow in the Tonga subduction zone back arc, *J. Geophys. Res.-Solid Earth*, 105(B7), 16,181-16,191.

Karato, S. (2007), *Deformation of Earth Materials: Introduction to the Rheology of the*

Solid Earth, Cambridge Univ. Press, New York, 462 pp.

Karato, S., and P. Wu (1993), Rheology of the upper mantle - a synthesis, *Science*, *260*(5109), 771-778.

Karato, S. I., and H. Jung (2003), Effects of pressure on high-temperature dislocation creep in olivine, *Philos. Mag.*, *83*(3), 401-414.

Karato, S. I., M. S. Paterson, and J. D. Fitz Gerald (1986), Rheology of synthetic olivine aggregates - influence of grain-size and water, *J. Geophys. Res.-Solid Earth and Planets*, *91*(B8), 8151-8176.

Karato, S., H. Jung, I. Katayama, and P. Skemer (2008), Geodynamic significance of seismic anisotropy of the upper mantle: New insights from laboratory studies, *Annual Review of Earth and Planetary Sciences*, *36*, 59-95.

Kato, T., G. S. El-Fiky, E. N. Oware, and S. Miyazaki (1998), Crustal strains in the Japanese islands as deduced from dense GPS array, *Geophys. Res. Lett.*, *25*(18), 3445-3448.

Khazaradze, G., and J. Klotz (2003), Short- and long-term effects of GPS measured crustal deformation rates along the south central Andes, *J. Geophys. Res.-Solid Earth*, *108*(B6), 2289, doi:10.1029/2002JB001879

Kincaid, C., and P. Olson (1987), An experimental-study of subduction and slab migration, *J. of Geophy. Res-Solid Earth and Planets*, *92*(B13), 13,832-13,840.

Kincaid, C., and R. W. Griffiths (2003), Laboratory models of the thermal evolution of the mantle during rollback subduction, *Nature*, *425*(6953), 58-62.

King, S. D., and B. H. Hager (1994), Subducted slabs and the geoid: Numerical

experiments with temperature-dependent viscosity, *J. Geophys. Res.-Solid Earth*, *99*(B10), 19,843-19,852.

King, S. D., A. Raefsky, and B. H. Hager (1990), ConMan - vectorizing a finite-element code for incompressible 2-Dimensional convection in the Earth's mantle, *Phys. Earth Planet. Inter.*, *59*(3), 195-207.

Kneller, E. A., P. E. van Keken, S. Karato, and J. Park (2005), B-type olivine fabric in the mantle wedge: Insights from high-resolution non-Newtonian subduction zone models, *Earth Planet. Sci. Lett.*, *237*(3-4), 781-797.

Lassak, T. M., M. J. Fouch, C. E. Hall, and E. Kaminski (2006), Seismic characterization of mantle flow in subduction systems: Can we resolve a hydrated mantle wedge?, *Earth Planet. Sci. Lett.*, *243*(3-4), 632-649.

Lee, C. Y., and S. D. King (2009), Effect of mantle compressibility on the thermal and flow structures of the subduction zones, *Geochem. Geophys. Geosyst.*, *10*, Q01006, doi:10.1029/2008GC002151.

Levin, V., and J. Park (1998), Quasi-Love phases between Tonga and Hawaii: Observations, simulations, and explanations, *J. Geophys. Res.-Solid Earth*, *103*(B10), 24,321-24,331.

Levin, V., D. Droznin, J. Park, and E. Gordeev (2004), Detailed mapping of seismic anisotropy with local shear waves in southeastern Kamchatka, *Geophys. J. Int.*, *158*(3), 1009-1023.

Lister, C. R. B. (1975), Gravitational drive on oceanic plates caused by thermal contraction, *Nature*, *257*(5528), 663-665.

Long, M. D., and R. D. van der Hilst (2005), Upper mantle anisotropy beneath Japan

from shear wave splitting, *Phys. Earth Planet. Inter.*, *151*(3-4), 206-222.

Long, M. D., and R. D. van der Hilst (2006), Shear wave splitting from local events beneath the Ryukyu arc: Trench-parallel anisotropy in the mantle wedge, *Phys. Earth Planet. Inter.*,*155*(3-4), 300-312.

Long, M. D., and P. G. Silver (2008), The subduction zone flow field from seismic anisotropy: A global view, *Science*, *319*(5861), 315-318.

Long, M. D., and T. W. Becker (2010), Mantle dynamics and seismic anisotropy, *Earth Planet.Sci. Lett.*, *297*(3-4), 341-354.

Long, M. D., H. Y. Gao, A. Klaus, L. S. Wagner, M. J. Fouch, D. E. James, and E. Humphreys (2009), Shear wave splitting and the pattern of mantle flow beneath eastern Oregon,*Earth Planet. Sci. Lett.*, *288*(3-4), 359-369.

Manea, V., and M. Gurnis (2007), Subduction zone evolution and low viscosity wedges and channels, *Earth Planet. Sci. Lett.*, *264*(1-2), 22-45.

Martinod, J., F. Funiciello, C. Faccenna, S. Labanieh, and V. Regard (2005), Dynamical effects of subducting ridges: insights from 3-D laboratory models, *Geophys. J. Int.*, *163*(3), 1137-1150.

McClusky, S., et al. (2000), Global Positioning System constraints on plate kinematics and dynamics in the eastern Mediterranean and Caucasus, *J. Geophys. Res.-Solid Earth*,*105*(B3), 5695-5719.

Mei, S., and D. L. Kohlstedt (2000), Influence of water on plastic deformation of olivine aggregates 1. Diffusion creep regime, *J. Geophys. Res.-Solid Earth*, *105*(B9), 21457-21469.

Moresi, L., and M. Gurnis (1996), Constraints on the lateral strength of slabs from three-

dimensional dynamic flow models, *Earth Planet. Sci. Lett.*, *138*(1-4), 15-28.

Moresi, L., and V. Solomatov (1998), Mantle convection with a brittle lithosphere: thoughts on the global tectonic styles of the Earth and Venus, *Geophys. J. Int.*, *133*(3), 669-682.

Moresi, L., M. Gurnis, and S. J. Zhong (2000), Plate tectonics and convection in the Earth's mantle: Toward a numerical simulation, *Comput. Sci. Eng.*, *2*(3), 22-33.

Nakajima, J., and A. Hasegawa (2004), Shear-wave polarization anisotropy and subduction-induced flow in the mantle wedge of northeastern Japan, *Earth Planet. Sci. Lett.*, *225*(3-4), 365-377.

Nicolas, A. and Christensen (1987), N. I., *Formation of anisotropy in upper mantle peridotites - A review, in Composition, struciure and dynamics of the lithosphere-asthenosphere system, 16,* 111-123, K. Fuchs and C. Froidevaux (Ed.), Washington, D.C. , AGU.

Nikolaeva, K., T. V. Gerya, and F. O. Marques (2011), Numerical analysis of subduction initiation risk along the Atlantic American passive margin, *Geology*, 39(5), 463–466.

Nataf, H. C., I. Nakanishi, and D. L. Anderson (1984), Anisotropy and shear-velocity heterogeneities in the upper mantle, *Geophys. Res. Lett.*, *11*(2), 109-112.

Piromallo, C., T. W. Becker, F. Funiciello, and C. Faccenna (2006), Three-dimensional instantaneous mantle flow induced by subduction, *Geophys. Res. Lett.*, *33*, *L08304*, doi:10.1029/2005GL025390.

Ranalli, G., (1995), *Rheology of the Earth* (2nd ed.), Chapman & Hall, London.

Ribe, N. M. (1989), Mantle flow induced by back arc spreading, *Geophys. J. Int.*, *98*(1),

85-91.

Ribe, N. M. (1992), On the relation between seismic anisotropy and finite strain, *J. Geophys. Res.-Solid Earth*, *97*(B6), 8737-8747.

Ribe, N. M., and Y. Yu (1991), A theory for plastic-deformation and textural evolution of olivine polycrystals, *J. Geophys. Res.-Solid Earth and Planets*, *96*(B5), 8325-8335.

Rowland, A., and J. H. Davies (1999), Buoyancy rather than rheology controls the thickness of the overriding mechanical lithosphere at subduction zones, *Geophys. Res. Lett.*, *26*(19), 3037-3040.

Russo, R. M., and P. G. Silver (1994), Trench-parallel flow beneath the nazca plate from seismic anisotropy, *Science*, *263*(5150), 1105-1111.

Savage, M. K. (1999), Seismic anisotropy and mantle deformation: What have we learned from shear wave splitting?, *Rev. Geophys.*, *37*(1), 65-106.

Savage, M. K., and A. F. Sheehan (2000), Seismic anisotropy and mantle flow from the Great Basin to the Great Plains, western United States, *J. Geophys. Res.-Solid Earth*, *105*(B6), 13,715-13,734.

Schellart, W. P. (2004), Kinematics of subduction and subduction-induced flow in the upper mantle, *J. Geophys. Res.-Solid Earth*, *109*, B07401, doi:10.1029/2004JB002970.

Schellart, W. P. (2005), Influence of the subducting plate velocity on the geometry of the slab and migration of the subduction hinge, *Earth Planet. Sci. Lett.*, *231*(3-4), 197-219.

Schellart, W. P., J. Freeman, D. R. Stegman, L. Moresi, and D. May (2007), Evolution

and diversity of subduction zones controlled by slab width, *Nature*, *446*(7133), 308-311.

Schmalholz, S. M. (2006), Scaled amplification equation: A key to the folding history of buckled viscous single-layers, *Tectonophysics*, *419*(1-4), 41-53.

Schmeling, H., and W. R. Jacoby (1981), On modeling the lithosphere in mantle convection with non-linear rheology, *Journal of Geophysics-Zeitschrift Fur Geophysik*, *50*(2), 89-100.

Schmeling, H., and G. Marquart (1991), The influence of 2nd-scale convection on the thickness of continental lithosphere and crust, *Tectonophysics*, *189*(1-4), 281-306.

Schmeling, H., et al. (2008), A benchmark comparison of spontaneous subduction models-towards a free surface, *Phys. Earth Planet. Inter.*, *171*(1-4), 198-223.

Schutt, D. L., and E. D. Humphreys (2001), Evidence for a deep asthenosphere beneath North America from western united states SKS splits, *Geology*, *29*(4), 291-294.

Sella, G. F., T. H. Dixon, and A. L. Mao (2002), REVEL: A model for recent plate velocities from space geodesy, *J. Geophys. Res.-Solid Earth*, *107*, 2081, doi:10.1029/2000JB000033.

Shearer, P. M., and J. A. Orcutt (1986), Compressional and shear-wave anisotropy in the oceanic lithosphere - the Ngendei seismic refraction experiment, *Geophysical Journal of the Royal Astronomical Society*, *87*(3), 967-1003.

Stegman, D. R., J. Freeman, W. P. Schellart, L. Moresi, and D. May (2006), Influence of trench width on subduction hinge retreat rates in 3-D models of slab rollback, *Geochem.Geophys. Geosyst.*, *7*, Q03012, doi:10.1029/2005GC001056.

Su, L. Q., and J. Park (1994), Anisotropy and the splitting of PS waves, *Phys. Earth*

Planet. Inter., *86*(4), 263-276.

Syracuse, E. M., P. E. van Keken, and G. A. Abers (2010), The global range of subduction zone thermal models, *Phys. Earth Planet. Inter.*, *183*(1-2), 73-90.

Tackley, P. J. (2000), Mantle convection and plate tectonics: Toward an integrated physical and chemical theory, *Science*, *288*(5473), 2002-2007.

Tackley, P. J., D. J. Stevenson, G. A. Glatzmaier, and G. Schubert (1994), Effects of multiple phase-transitions in a 3-dimensional spherical model of convection in earths mantle, *J.Geophys. Res.-Solid Earth*, *99*(B8), 15,877-15,901.

Tao, W. C., and R. J. O'Connell (1993), Deformation of a weak subducted slab and variation of seismicity with depth, *Nature*, *361*(6413), 626-628.

Taylor, B., and G. D. Karner (1983), On the evolution of marginal basins, *Rev. Geophys.*, *21*(8), 1727-1741.

Thoraval, C., and M. A. Richards (1997), The geoid constraint in global geodynamics: viscosity structure, mantle heterogeneity models and boundary conditions, *Geophys. J. Int.*, *131*(1), 1-8.

Vassiliou, M. S., B. H. Hager, and A. Raefsky (1984), The distribution of earthquakes with depth and stress in subducting slabs, *J. Geodyn.*, *1*(1), 11-28.

Vlaar, N. J., and M. J. R. Wortel (1976), Lithospheric aging, instability and subduction, *Tectonophysics*, *32*(3-4), 331-351.

Wilson, M. (1993), Plate-moving mechanisms - constraints and controversies, *J. Geol. Soc.*, *150*, 923-926.

Wolfe, C. J., and S. C. Solomon (1998), Shear-wave splitting and implications for mantle

flow beneath the MELT region of the East Pacific Rise, *Science*, *280*(5367), 1230-1232.

Wenk, H. R., G. Canova, A. Molinari, and U. F. Kocks (1989), Viscoplastic modeling of texture development in quartzite, *J. Geophys. Res.-Solid Earth and Planets*, *94*(B12), 17895-17906.

Xue, M., and R. M. Allen (2005), Asthenospheric channeling of the Icelandic upwelling: Evidence from seismic anisotropy, *Earth Planet. Sci. Lett.*, *235*(1-2), 167-182.

Zhang, S. Q., and S. Karato (1995), Lattice preferred orientation of olivine aggregates deformed in simple shear, *Nature*, *375*(6534), 774-777.

Zhong, S. J., and M. Gurnis (1992), Viscous-flow model of a subduction zone with a faulted lithosphere - long and short wavelength topography, gravity and geoid, *Geophys. Res. Lett.*, *19*(18), 1891-1894.

Zhong, S. J., and M. Gurnis (1995), Mantle convection with plates and mobile, faulted plate margins, *Science*, *267*(5199), 838-843.

Zhong, S. J., and M. Gurnis (1996), Interaction of weak faults and non-newtonian rheology produces plate tectonics in a 3D model of mantle flow, *Nature*, *383*(6597), 245-247.

Zhong, S. J., M. Gurnis, and L. Moresi (1998), Role of faults, nonlinear rheology, and viscositystructure in generating plates from instantaneous mantle flow models, *J. Geophys. Res.-Solid Earth*, *103*(B7), 15,255-15,268.

Zhong, S. J., A. McNamara, E. Tan, L. Moresi, and M. Gurnis (2008), A benchmark

study on mantle convection in a 3-D spherical shell using CitcomS, *Geochem. Geophys. Geosyst., 9*, Q10017, doi:10.1029/2008GC002048

Figure 1.1. Isotropic and Anisotropic Wave Propagation

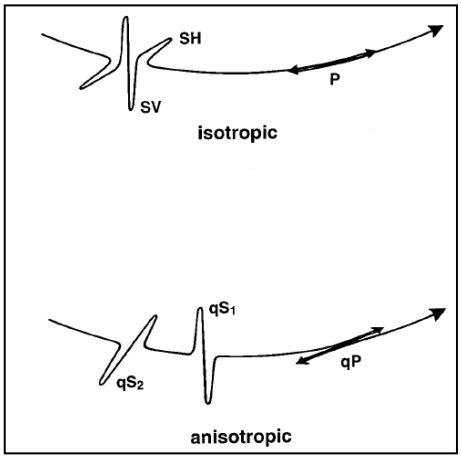

The isotropic and anisotropic wave propagation, in three dimensional space. The quasi S wave propagation directions ($qS_1$and qS_2) polarizations are parallel and perpendicular to the fast direction for the propagation direction in question, from Savage, M. K. (1999), Seismic anisotropy and mantle deformation: What have we learned from shear wave splitting?, *Rev. Geophys., 37*(1), 65-106. (Used under fair use guidelines, 2012).

Figure 1.2. Compilation of Shear Wave Splitting Observations Around Pacific Rim

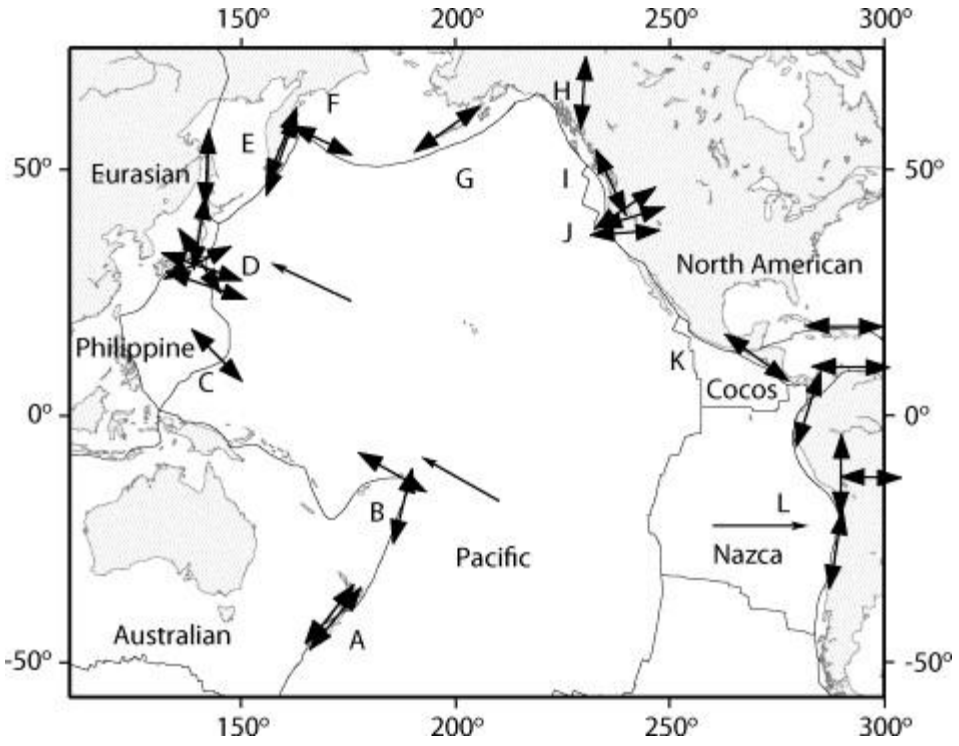

Compilation of shear wave splitting observations around the Pacific Rim from Lassak, T. M., M. J. Fouch, C. E. Hall, and E. Kaminski (2006), Seismic characterization of mantle flow in subduction systems: Can we resolve a hydrated mantle wedge?, *Earth Planet. Sci. Lett., 243*(3-4), 632-649. The fast polarization directions are observed along the subduction region. Both trench –parallel and trench perpendicular strike directions are observed. The double headed arrow indicates the average regional orientation of the fast polarization direction. (Used under fair use guidelines, 2012).

Figure 1.3. Compilation of Convergence Velocity and Trench-migration Velocity of Various Subduction Zones of the World

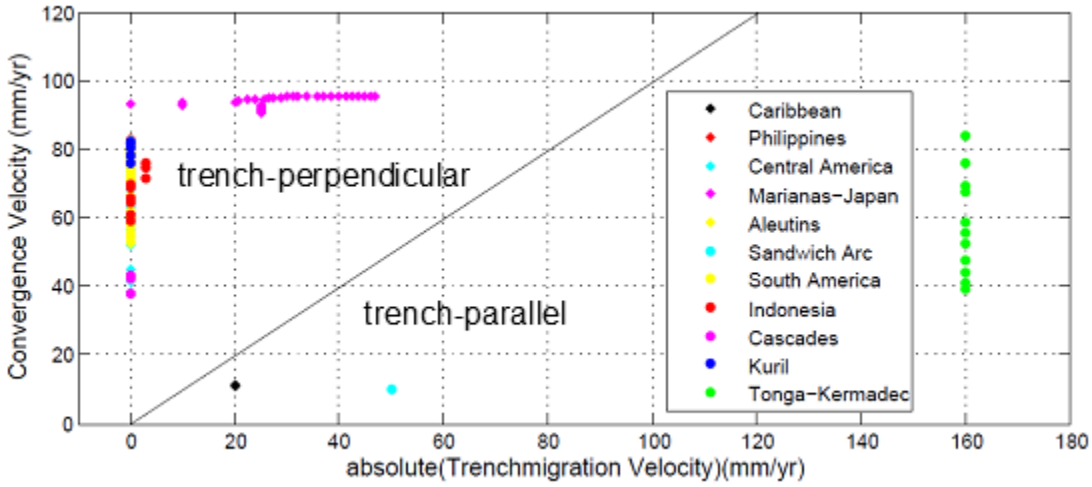

Plot showing division of subduction regions of the world based on trench-perpendicular vs. trench-parallel flow pattern. Data taken from Cruciani, C., E. Carminati, and C. Doglioni (2005), Slab dip vs. lithosphere age: No direct function, *Earth Planet. Sci. Lett.*, *238*(3-4), 298-310. (Used under fair use guidelines, 2012).

Figure 1.4. Flow Diagram Modified from Long and Silver (2008)

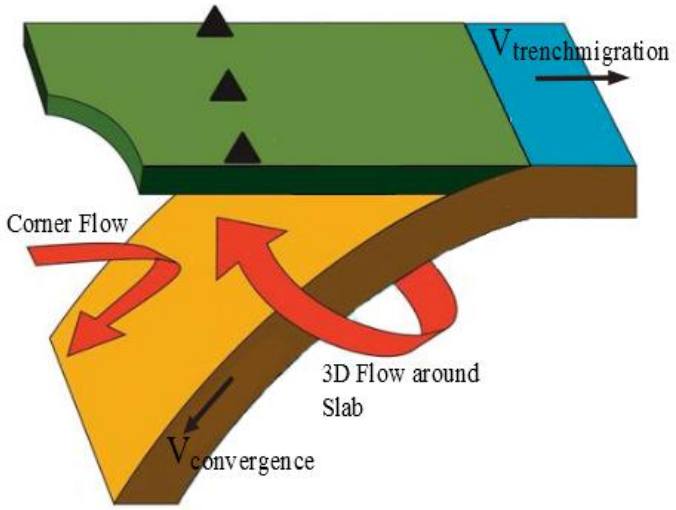

A diagram modified from Long, M. D., and P. G. Silver (2008), The subduction zone flow field from seismic anisotropy: A global view, *Science*, *319*(5861), 315-318, that shows the dominant 3D flow beneath the slab and the 2D corner flow in the mantle wedge region. (Used under fair use guidelines, 2012).

CHAPTER 2: METHODS

2.1. Governing Equations

In the present study the mantle is treated as an anelastic and incompressible viscous fluid. Like most mantle convection problems Prandtl number is close to infinity (Turcotte and Oxburg ,1967) with a very low dissipation number (King et al., 2010). The finite element method is used to find the solution for velocity and temperature using an the code Citcoms (Zhong et al., 2000; Tan et al., 2006). The three basic equations used to calculate the fluid motions are:

Continuity equation:

$$\nabla \cdot \vec{u} = 0 \tag{1}$$

Conservation of momentum:

$$-\nabla P + \nabla \cdot \left[\eta(\nabla \vec{u} + \nabla^T \vec{u})\right] + Ra\Delta T\delta_{ir} \tag{2}$$

Conservation of energy:

$$(\frac{\partial T}{\partial t} + \vec{u} \cdot \nabla T) = \nabla \kappa \nabla T \tag{3}$$

where u is the velocity, P is the pressure , η is the viscosity, T is the temperature δ_{ir} is the Kroneker delta tensor where i and r are the spatial indices in the longitudinal and radial directions. Phase changes and internal heating are not considered in this problem.

The thermal Rayleigh number is given by,

$$Ra = \frac{\rho_0 g \alpha_0 \Delta T R_0^{\ 3}}{\kappa_0 \eta_0} \qquad (4)$$

where ρ_0, α_0, η_0, and κ_0 are the reference density, thermal expansivity, viscosity and thermal diffusivity values which are chosen at the bottom of the mantle. The acceleration due to gravity is g and R_0 is the radius of the Earth. ΔT is defined as the temperature drop from the core-mantle boundary (CMB) to the surface. The Rayleigh number is a factor of eight higher in comparison to most previous studies of mantle convection because in CitcomS the radius of the Earth is considered rather than the depth of the convecting layer.

2.2 Model Domain

The model domain is a 3-D segment of a spherical shell that extends to a depth of 1500 km. The aim of the study is to formulate a self-consistent subduction zone without imposing surface velocity conditions and/or weak zones to observe the horizontal to vertical flow pattern. The model is made as simple as possible and complications due to the presence of an overriding plate are avoided. The bottom of the model domain is isothermal set to non-dimensionalised temperature of 1. The model domain is divided into a subducting plate at the surface and a constant temperature region next to it. The subducting plate is fixed at one end and a constant plate velocity of 5 cm/yr is applied to it. To keep the model simple no overriding plate is modeled following the geometry used

in Schmelling et al. (2008). The mesh element size along both the directions is a constant 46.15 km along the colatitude and longitude directions. The length of the model domain is 3000 km in both colatitude and longitude directions (Figure 2.1). Along the depth of the model the grid element size is 23 km. The age of the subducting plate varies from 0 Ma at the model domain boundary to 40 Ma, 80 Ma and 120 Ma respectively at the plate boundary. The model grid contains $65X65X65$ finite elements nodes in the longitudinal, latitudinal, and radial directions with a total of 262144 elements. Figure 2.1 is an illustration of the model domain along with grid spacing.

2.3. Initial Thermal Structure

The initial thermal model is constructed by using a semi-infinite half space cooling model (Turcotte and Schubert, 2002). The thickness of the thermal boundary layer can be given in terms of plate age by the following equation:

$$T = (T_0 - T_1)erfc(\frac{r}{2\sqrt{\kappa t}}) + T_1 \qquad (5)$$

where r is the dimensionalized radial distance, t is the age of the plate, T_0 is the non-dimensionalized surface temperature and T_1 is the non-dimensionalized temperature of mantle and κ is the thermal diffusivity. The initial ranges of ages for the plate are chosen to be 40 Ma, 80 Ma and 120 Ma respectively. The age of subducting plate varies from 0 at the model domain boundary 40 Ma, 80 Ma and 120 Ma respectively at the subduction zone. The temperature profile along the inflow/outflow boundary of the mantle wedge is prescribed to be non-dimensionalized temperature of 1. The temperature

of the top surface of the box is fixed as 0. Figure 2.2 is the initial temperature structure of the subduction model.

2.4. Rheology

In this study a temperature and stress dependent viscosity is considered. The advantage of using temperature dependent viscosity is that it introduces heterogeneity to the mantle that is close to realistic situation (van Keken and Ballentine, 1999). Olivine is the most abundant mineral in the upper mantle (Bodinier and Godard, 2003) and the properties of olivine controls most of the stress dependent parameters. Hence to understand the upper mantle rheology it is important to understand the properties of olivine. Because the upper mantle has both cold subducting lithosphere as well as the hot convecting mantle the physical properties of olivine widely vary. Two creep mechanisms have been observed in laboratory study of olivine these are the diffusion creep and the dislocation creep. Hirth and Kohlstedt (2003) showed in laboratory studies that the deformation of olivine occurs both by diffusion and dislocation creep mechanism. Diffusion creep is a mechanism of plastic deformation in polycrystalline materials at low stress and small grain size. At high temperature atoms move from their stable position and diffuse out with some probability due to thermally processes. In diffusion of atoms and vacancies through lattice then the relation of strain rate to stress is linear and is known as Newtonian or linear relationship. The other type of creep is the dislocation creep which is dominant in earth under conditions of high stress. This creep mechanism depends on the grain size and hence is also stress dependent or non-Newtonian. Non-Newtonian may also result due to dislocation of grains Weertman and Weertman (1975).

In dislocation creep the dislocation density increases with applied stress and dislocation velocity also increases with stress (Karato, 2007). Diffusion creep dominates at relatively small grain size and low stress (Cooper and Kohlstedt, 1984; Karato et al., 1986; Hirth and Kohlstedt, 1995a) whereas dislocation creep is observed at higher stresses (Durham and Goetze, 1977; Karato et al., 1986; Hirth and Kohlstedt, 1995b). Laboratory experiments have been performed to determine the deformation mechanism due to the effect of temperature, stress and grain size (Frost and Ashby, 1982). The dominant slip plane of olivine (010) crystallographic axis is very sensitive to presence of water (Katayama et al., 2004) and pressure (Mainprice et al., 2005) and high differential stresses (Faul et al., 2011).

Andrew and Billen (2009) argued that due to dislocation creep, the slabs gets detached due to buoyancy differences and certain regions have high strain rate that reduces the mantle viscosity and provides less viscous support to the slab than diffusion creep.

2.4.1. Temperature and Stress Dependent Viscosity

The viscosity of the mantle is strongly temperature dependent regardless of subsolidus deformation processes (Turcotte and Schubert, 2002). But the effective viscosity of the mantle will also be stress dependent considering presence of creep mechanism especially the dislocation creep mechanism. Chen and King (1998) studied geoid and topography and compared it with observed topography in subduction region. Their study reveals that viscosity of the lower mantle is important in controlling the width of trench. They stated that for both depth dependent as well temperature dependent

viscosity the lower mantle viscosity should be a minimum of 10-30 times higher than the upper mantle viscosity for geoid profile to be close to observed geoid profile. In the finite element numerical convection code CitcomS, used in this study, the built-in non-dimensionalized viscosity η formulation is used:

$$\eta = \eta(r)\exp\left[\frac{E_\eta + V_\eta(1-r)}{T+T_s} - \frac{E_\eta + V_\eta(1-r_{core})}{1+T_s}\right] \quad (6)$$

η(r) is a term that varies with radial viscosity profile and also depends on the layering of the mantle. A two layered mantle model is used in this case. E_η and V_η are the normalized activation energy and activation volume respectively and are same as the normalized parameters are same as used by (Roberts and Zhong, 2006)

$$E_\eta = \frac{E}{R\Delta T} \quad (7)$$

$$V_\eta = \frac{\rho_0 g R_0 V}{R\Delta T} \quad (8)$$

$$T_s = \frac{T_{surf}}{\Delta T}. \quad (9)$$

In this study we are concerned with only the temperature dependent viscosity effect, so we have removed the pressure dependent viscosity which depends on the radius and the equation (1) reduces to

$$\eta = \eta(r)\exp\left[\frac{E_\eta}{T+T_s} - \frac{E_\eta}{1+T_s}\right] \quad (10)$$

The above equation (10) was used for a two-layer mantle where the ratio of the $\eta_{lower}/\eta_{upper}$ is 30.

Mantle deformation is complex and includes brittle-ductile and viscous behavior (Kohlstedt et al., 1995). The brittle-ductile deformation is can be approximated using a yield stress (Tackley, 2000; Billen and Hirth, 2007; Lee and King, 2011). Karato and Li (1992) have shown that both linear and non-linear creep mechanisms are significant processes in mantle flow. The interior of the earth can be divided into four regimes in terms of creep mechanism: 1) diffusion creep at low stress and small grain size (Karato et al., 1986; Hirth and Kohlstedt, 1995a); 2) dislocation creep at higher stress (Karato et al., 1986; Hirth and Kohlstedt,1995b); 3) a transition region in grain size and stress between diffusion creep and dislocation creep termed dislocation assisted grain boundary sliding (Hirth and Kohlstedt, 1995b and 2003); 4) low-temperature plasticity thought to apply at low temperatures and high stresses (Hirth and Kohlstedt , 2003). Laboratory experiments show that dislocation creep and diffusion creep are dominant in the upper mantle but in the lower mantle is dominantly diffusion creep (Billen and Hirth, 2007; Hirth and Kohlstedt, 2003).

Dislocation and diffusion creep are described below in terms of activation energy and activation volume as:

$$\eta_{dif} = A_{dif}^{-1} d_g^{m} \exp\left[\frac{E_{dif} + PV_{dif}}{RT}\right] \tag{11}$$

$$\eta_{dis} = A_{dis}^{-1/n} \exp\left[\frac{E_{dis} + PV_{dis}}{RT}\right]^{\frac{1-n}{n}} \dot{\varepsilon}_S \tag{12}$$

where A is a prefactor, E is the activation energy, V is the activation volume, d is the grain size n is the stress exponent and m is the grain size exponent and R is the gas constant.

In case of a Newtonian mantle (i.e., diffusion creep) the gravitational body force pulling the slab into the mantle is largely resisted locally by frictional forces on the upper and lower surfaces of the slab (Tovish and Schubert, 1978). Whereas, with a non-Newtonian rheology (i.e., dislocation creep) in the upper mantle decreases viscous resistance around the slab allowing it to deform more freely in the upper mantle (Billen and Hirth, 2007).

The behavior of non-Newtonian rheology in modification of effectively mantle viscosity can be expressed as in a generalalized form in the built-in non-dimensionalized viscosity η formulation in CitcomS. Assuming a general form of the viscosity equation with constant stress and $\dot{\varepsilon}$ as the second derivative of strain rate, the equation can be given as:

$$\eta = \dot{\varepsilon}_{II}^{\frac{1-n}{n}} \eta(r) \exp\left[\frac{E_\eta}{T+T_s} - \frac{E_\eta}{1+T_s}\right] \tag{13}$$

Where $\dot{\varepsilon}_{II}$ is the second invariant of strain rate tensor given by:

$$\dot{\varepsilon}_{II} = \left(\dot{\varepsilon}_{ij}^2 / 2\right)^{1/2} \tag{14}$$

E_η and T_S is the activation energy and temperature field defined by convective flow respectively. n is the stress exponent and changes depending on dislocation and diffusion creep.

2.4.2 Sticky Air Layer

The Earth's surface can be considered as a free surface that is laterally as well as vertically unconstrained and can adjust to any forces (OzBench et al., 2008). The Earth's surface is naturally stress-free boundary and dynamically responds to variations in surface and subcrustal loads (Gurnis et al., 1996). If the upper part of the Earth surface is modeled as a free surface then the free surface enhances the vertical flow in the mantle interior and this influences the mantle temperature field, especially in the shallow part of the mantle structure. To mimic the free surface boundary of the Earth a low viscosity "sticky air" layer is introduced at the top of the model. Self-consistent subduction with sticky air region has been modeled by Morra et al. (2007), Ozbench et al. (2008) and Schmeling et al. (2008). Is has been observed by Schmeling et al. (2008) and Sizova et al. (2010) that the large viscosity contrast caused by the low viscosity boundary layers minimizes shear stresses ($>10^4$Pa) at the top of the lithosphere making it an efficient free surface. In the present approach a thin "sticky air" layer which is impermeable and free of shear traction and has a low viscosity and zero activation energy is considered. In this low-viscosity layer the normal stresses are greater than the shear stresses (Gurnis et al., 1996). The purpose of the sticky air layer is to lubricates and decouple the slab from the surface in a self-consistent way (Schmeling et al. 2008). In the model the resolution of the sticky air layer is approximately ~60 km; this is the minimum resolution possible to get with the present grid size and is about 3 elements thick along the radial direction. The introduction of the sticky-air layer makes the rheology weak by decreasing the effective viscosity above the downgoing slab (Schmeling et al., 2008). The geophysical significance of the subduction of a weak sticky air layer is discussed by Gerya et al.

(2002) and Gerya and Yuen (2003b). During subduction water rich oceanic crust or sediments may produce a several km thick weak serpenthenized subduction channel on top of the subducting slab similar to sticky air layer. Hence mimicking the free surface by a weak layer might indeed lead to a rheologically reasonable scenario.

2.5. Velocity Boundary Conditions

The model uses Eulerian framework and the top of surface is free-slip boundary condition. The sides of the model domain are reflecting or free-slip boundary condition. The sidewall boundary a free-slip creates a reference frame for motion of the system that will be fixed to the model domain. In an ideal subduction situation the difference in buoyancy between the slab and the mantle is the driving force with no imposed surface velocity conditions. A free-slip boundary condition is implemented at the bottom of model domain. The mantle and the subducting slab are fully coupled so the velocity of mantle beneath the slab is same as the velocity of the slab. A constant velocity of 5 cm/yr is applied to the subducting plate and 2 cm/yr to the overriding plate region (Figure 2.4).

In the present model a threefold approach is used. Case 1: Imposed velocity conditions to the subducting and the overriding plate region. The top of the model domain has tangential surface velocity conditions specified by the plate velocities Case 2: Imposed velocity condition with trench migration velocity to observe trench migration (Figure 2.5) and finally Case 3: Self-consistent subduction with sticky air layer. To initiate the subduction imposed plate velocity is applied for 5 Ma and then the stick air layer is introduced and the model is allowed to subduct on its own.

To calculate relative plate velocities it is important to know the instantaneous rotation pole and angular velocity for a pair of adjacent plates. The figure taken from Fowler (1990) explains the different parameters are required to calculate the plate geometry. The pole of rotation for the plates (Fowler, 1990) are chosen such that the velocity vectors are almost parallel to the boundary of the model domain, hence the physical location of the poles are far away from the model space. The plate velocity parameters a and C as is shown in Figure 2.3 can be calculated by:

$$\cos a = \cos(90-\theta)\cos(90-\theta') + \sin(90-\theta)\sin(90-\theta')\cos(\psi-\psi') \quad (15)$$

$$C = \sin^{-1}\left(\frac{\cos(\theta'\sin(\psi-\psi')}{\sin a}\right) \quad (16)$$

where θ, θ' are the latitude of the location and the pole respectively. Whereas, ψ and ψ' are the longitude of location and the pole respectively. The velocity of the plate is given by:

$$v = \omega R \sin a \quad (17)$$

where ω is the angular velocity and R is the radius of the Earth.

2.6. Seismic Anisotropy Model

The crystallographic orientation of grains in a polycrystalline material may be non-random. This non-random distribution of crystallographic axes orientation is called Lattice Preferred Orientation (LPO). LPO develops due to deformation such as compression and dislocation glide. At low temperature the crystallographic orientation for all the grains remains the same (Karato, 2008), but at high temperature deformation of grain can be heterogeneous which can cause grain size reduction, grain boundary

migration and grains with selective nucleation. This phenomenon is known as dynamic recrystallization (Karato, 2008). Because olivine is the most abundant mineral on the upper mantle, the evolution of LPO in olivine can occur by both dynamic re-crystallization and inter-crystalline slip (Kaminski and Ribe, 2001). A model was developed by Kaminski and Ribe (2001; 2002) to predict the LPO evolution in olivine aggregate by plastic deformation and dynamic recrystallization.

The plastic deformation as individual grains of each mineral phase responds aggregately by imposed deformation by combination of rigid body rotation and simple shear on independent slip system (Ribe and Yu, 1991). Each of the minerals obeys a power law rheology and activation stress and stress exponent. The deformation gradient d_{ij}^{ν} for each crystal υ can be written in terms of velocity gradient tensor as:

$$d_{ij}^{\nu} = G_{ij}^{\nu}\gamma^{\nu} - \varepsilon_{ijk}\omega_k^{\nu} \tag{18}$$

where ω_k is the rotation rate of crystallographic axes and γ^{ν} is the rate of slip on the weakest slip plane, ε_{ijk} is the strain rate. G_{ij}^{ν} is the Schmidt tensor which is defined for S slip system as:

$$G_{ij}^{\nu} = \sum_{S=1}^{S} \beta_m^{S\nu} l_i^{S\nu} n_j^{S\nu} \tag{19}$$

where $l_i^{S\nu}$ and $n_j^{S\nu}$ are unit vectors in slip direction and normal to the slip and $\beta_m^{S\nu}$ can be written as:

$$\beta_m^{S\nu} = \frac{\tau_O I^{S\nu}}{\tau_m^S I^{1\nu}} \left| \frac{\tau_O I^{S\nu}}{\tau_m^S I^{1\nu}} \right|^{n-1} \tag{20}$$

where , $I^{Sv} = l_i^{Sv} n_j^{Sv} E_{ij}$ and E_{ij} is the macroscopic strain rate and τ_O is the reference activation stresses , τ_m^S is the activation stress of the Sth slip plane and n is the stress exponent.

If there is an externally imposed velocity gradient tensor then the deformation of the crystals is function of orientation and the ratio $\frac{\tau_O}{\tau_m^S}$ for shear plane of different phases. The quantities γ^v and ω_k^v are calculated by minimizing the difference between the global velocity gradient tensor and the local velocity gradient tensor.

Dynamic recrystallization is a complex process that is associated with changes in microstructure crystallographic orientation and rheological properties. Dynamic recrystallization is associated with stored energy. If a crystal has high strain energy then it is invaded by crystal with low energy through grain boundary migration.

The equation for stored strain energy is given as:

$$E = A\rho\mu b^2 \qquad (21)$$

where A is a dimensionless constant, ρ is the dislocation density, b in the length of the Burger's vector and μ is the shear modulus.

If there is a large change in thermodynamic parameters then phase transformation occurs through localized atomic motion involving nucleation. Nucleation occurs by sub-grain rotation, grain boundary bulging and creating strain free zones in the parent grain. Introduction "nucleation parameter" λ, to stored strain energy the equation (23) modifies to:

$$E = \alpha A\rho\mu b^2 \qquad (22)$$

where α is the non-recrystallized fraction of the grain and is given by:

$$\alpha = \exp\left[-\lambda\rho^2\right] \tag{23}$$

When plastic deformation is combined with dynamic recrystallization then the relation between densities of dislocation (deformation) ρ^S on a slip on a slip plane S to crystal deformation with shear stress τ^S and can be related to power law as:

$$\frac{\rho^S}{\rho^S_{ref}} \equiv \left(\frac{\tau^S}{\tau^S_{ref}}\right)^p \equiv \left|\frac{\dot{\varepsilon}^S}{\dot{\varepsilon}_{ref}}\right| \tag{24}$$

The total stored strain energy in a grain can be expressed as a function of different slip systems:

$$E = A\mu b^2 \sum_S \rho^S_{ref} \left|\frac{\dot{\varepsilon}^S}{\dot{\varepsilon}_{ref}}\right|^{p/n} \exp\left[-\lambda\left(\rho^S_{ref}\left|\frac{\dot{\varepsilon}^S}{\dot{\varepsilon}_{ref}}\right|^{p/n}\right)^2\right] \tag{25}$$

The above equations (24) and (25) are determined in terms of a reference state for crystal such that reference shears stress τ^S_{ref} on slip system S corresponds to shear rate $\dot{\varepsilon}_{ref}$ on that slip system. The reference density of dislocation is ρ^S_{ref} on the slip system S and p is an exponent that depends on temperature.

The lattice preferred orientation due to plastic and dynamic recrystallization depends on the initial lattice preferred orientation of the aggregate and deformation history (Kaminski and Ribe , 2002). The LPO orientation of an olivine aggregate in simple shear follows a finite strain ellipsoid pattern and tends to rotates rapidly towards the shear plane.

As an example of lattice preferred orientation towards finite strain ellipsoid Kaminski and Ribe (2002) showed the following problem for a vorticity number Γ and then determining ψ_{FSE} orientation of the long axis of finite strain ellipse:

$$\psi_{FSE} = \frac{1}{2}\tan^{-1}\left[\frac{\Gamma \tanh\left(\sqrt{1-\Gamma^2}\dot{\varepsilon}t\right)}{\sqrt{1-\Gamma^2}}\right] \quad (26)$$

where $\dot{\varepsilon}$ is the strain rate and t is the time. When $t \to \infty$ then the asymptotic orientation of the long axis of the finite strain ellipsoid corresponds to the steady state a-axis orientation of olivine. The long axis orientation is called the infinite strain axis (ISA) and the above equation will change to $\psi_{ISE} = \frac{1}{2}\sin^{-1}\Gamma$ and is independent of time.

Kaminski and Ribe (2002) also showed that the time scale for ISA development depends on flow field but can be approximated as $\tau_{ISA} \sim \dot{\varepsilon}^{-1}$ where $\dot{\varepsilon}$ is the absolute value for the largest eigen vector. It can also depend on vorticity vector and orientation of vorticity vector relative to principle strain rate axis. So rate at which the LPO rotates toward the ISA can be estimated by $\Omega_{ISA} \sim \dot{\varepsilon}$. However when olivine aggregates are advected through mantle the velocity gradient tensor may vary spatially and the orientation ISA may experience temporal changes (Conrad et al., 2007). Kaminski and Ribe (2001) introduced the term on the rate of ISA orientation along flow line Ω_{flow} which is the angle between the local flow direction and local ISA. Based on Ω_{flow} and Ω_{ISA}, two situation can arise in a spatially changing velocity gradient field; case 1: $\Omega_{flow} > \Omega_{ISA}$ then the net LPO development will depend on strain history in a complex

way and case 2: $\Omega_{flow} < \Omega_{ISA}$ where the LPO approaches ISA orientation. To determine the rate of formation of Ω_{flow} and Ω_{ISA} a non- dimensionless term called the "grain orientation lag" was introduced by Kaminski and Ribe (2002) which this is given as:

$$\Pi \equiv \frac{\Omega_{flow}}{\Omega_{ISA}} \quad . \tag{27}$$

The GOL describes the rate of change of the infinite strain axis orientation along a pathline. If the rate of change is slow enough then LPO directions adjust to it, following

$$\Omega_{flow} = \frac{D\Theta}{Dt} = \frac{\partial\Theta}{\partial t} + u.\nabla\Theta \quad , \tag{28}$$

where Θ is the angle between the flow direction u and ISA. The first term on the right hand side is equation (28) is the time dependence of flow field, while the second term represents the change in Θ as grains are advected along flow lines and is determined from the velocity field and the ISA direction. The advective and density driven time dependent changes in Θ are used in calculation of Ω_{flow}. The time dependent changes for plate dependent flow are negligible and are not considered. The 2D DRex Code modified by Kaminski and Ribe (2001), Kaminski and Ribe (2002) and Kaminski et al. (2004) uses all these parameters and calculate LPO direction from mantle flow directions. The 2D code was further modified by Conrad et al. (2007) and Conrad and Behn (2010) to work with spherical coordinates and 3D CitcomS.

The simplest asthenospheric flow is the shear flow (Figure 2.6). With more stress parameters such as high stress environment or water rich environment different types of asthenospheric fabrics are generated and are not always parallel to the maximum shear

stress direction. The asthenospheric flow is decomposed into mantle flow, flow driven by relative plate motions and net rotation of the lithosphere (Conrad and Behn, 2010).

References

Andrews, E. and M. I. Billen (2009) Rheologic Controls on Slab Detachment, *Tectonophysics, Special Volume on Slab Detachment*, 464, 60-69.

Batchelor, G. K., (1967), *An Introduction to Fluid Dynamics,Cambridge Univ. Press*, New York.

Becker, T.W., C. Faccenna (2009), A review of the role of subduction dynamics for regional and global plate motions, Lallemand, S., Funiciello, F. (eds.,) *Subduction Zone Geodynamics*, doi: 10.1007/978-3-540-87974-9, Springer-Verlag Berlin HeidelbergSpringer, 3–34.

Billen, M. I., and G. Hirth (2007), Rheologic controls on slab dynamics, *Geochem. Geophys.Geosyst., 8*, Q08012, doi:10.1029/2007GC001597.

Bodinier, J. L. & Godard, M. (2003), Orogenic, ophiolitic, and abyssal peridotites. In: Carlson, R. W. (ed.) Treatise on Geochemistry (vol 2.), *Geochemistry of the Mantle and Core,* Amsterdam: Elsevier, 103-170

Chen, J. N., and S. D. King (1998), The influence of temperature and depth dependent viscosity on geoid and topography profiles from models of mantle convection, *Phys. Earth Planet. Inter.*, *106*(1-2), 75-92.

Conrad, C. P., and M. D. Behn (2010), Constraints on lithosphere net rotation and asthenospheric viscosity from global mantle flow models and seismic anisotropy,

Geochem. Geophys Geosyst., *11*, Q05W05, doi:10.1029/2009GC002970.

Conrad, C. P., M. D. Behn, and P. G. Silver (2007), Global mantle flow and the development of seismic anisotropy: Differences between the oceanic and continental upper mantle, *J. Geophys. Res.-Solid Earth*, *112*, B07317, doi:10.1029/2006JB004608.

Cooper, R. F., and D. L. Kohlstedt (1984), Solution-precipitation enhanced diffusional creep ofpartially molten olivine-basalt aggregates during hot-pressing, *Tectonophysics*, *107*(3-4), 207-233.

Durham, W. B., and C. Goetze (1977), Plastic-flow of oriented single-crystals of olivine .1. Mechanical data, *Journal of Geophysical Research*, *82*(36), 5737-5753.

Faul, U. H., J. D. F. Gerald, R. J. M. Farla, R. Ahlefeldt, and I. Jackson (2011), Dislocation creep of fine-grained olivine, *J. Geophys. Res.-Solid Earth*, *116*, B01203, doi:10.1029/2009JB007174

Frost, H. J., F. Spaepen, and M. F. Ashby (1982), a 2nd report on tilt boundaries in hard-sphere fcc crystals, *Scripta Metallurgica*, *16*(10), 1165-1170.

Fowler, C.M.R. (1990), *The solid Earth, an Introduction to Global Geophysics, Cambridge Univ. Press*, Cambridge.

Gerya, T. V., and D. A. Yuen (2003b), Characteristics-based marker-in-cell method with conservative finite-differences schemes for modeling geological flows with strongly variable transport properties, *Phys. Earth Planet. Inter.*, *140*(4), 293-318

Gerya, T. V., L. L. Perchuk, W. V. Maresch, A. P. Willner, D. D. Van Reenen, and C. A. Smit (2002), Thermal regime and gravitational instability of multi-layered

continental crust: implications for the buoyant exhumation of high-grade metamorphic rocks, *Eur. J. Mineral.*, *14*(4), 687-699.

Gurnis, M., C. Eloy, and S. J. Zhong (1996), Free-surface formulation of mantle convection .2 Implication for subduction-zone observables, *Geophys. J. Int.*, *127*(3), 719-727.

Hirth, G., and D. L. Kohlstedt (1995a), Experimental constraints on the dynamics of the partially molten upper mantle: Deformation in the diffusion creep regime, *J. Geophys. Res.*, 100(B2), 1981–2001.

Hirth, G., and D. L. Kohlstedt (1995b), Experimental constraints on the dynamics of the partially molten upper mantle: 2. Deformation in the dislocation creep regime, *J. Geophys. Res.* 100(B8), 15,441–15,449.

Hirth, G., and D. L. Kohlstedt (2003), Rheology of the upper mantle and the mantle wedge: A view from the experimentalists, In J. Eiler (Ed.), *Inside the Subduction Factory*, Geophys. Monogr.(vol. 138), AGU, Washington, D. C., 83–105.

Mainprice, D., A. Tommasi, H. Couvy, P. Cordier, and D. J. Frost (2005), Pressure sensitivity of olivine slip systems and seismic anisotropy of Earth's upper mantle, *Nature*, *433*(7027), 731-733.

McKenzie, D.P.(1967), Some remarks on heat flow and gravity anomalies. *J. Geophys. Res.*, *72,* 6261-6273.

Morra, G., Chatelain, P., Tackley, P. and P. Koumoutsakos (2007), Large scale three-dimensional boundary element simulation of subduction, *Int. Conf.Comp. Sci.*, Part III, *4489*, 1122–1129.

Kaminski, E., and N. M. Ribe (2001), A kinematic model for recrystallization and texture

development in olivine polycrystals, *Earth Planet. Sci. Lett.*, *189*(3-4), *253-267.*

Kaminski, E., and N. M. Ribe (2002), Timescales for the evolution of seismic anisotropy in mantle flow, *Geochem. Geophys. Geosyst.*, 3(8), 1051, doi:10.1029/2001GC000222.

Kaminski, E., N. M. Ribe, and J. T. Browaeys (2004), D-rex, a program for calculation of seismic anisotropy due to crystal lattice preferred orientation in theconvective upper mantle, Geophys. J. Int., 158, 744 – 752.

King, S. D., C. Lee, P. E. van Keken, W. Leng, S. J. Zhong, E. Tan, N. Tosi, and M. C. Kameyama (2010), A community benchmark for 2-D Cartesian compressible convection in the Earth's mantle, *Geophys. J. Int.*, *180*(1), 73-87.

Katayama, I., H. Jung, and S. I. Karato (2004), New type of olivine fabric from deformation experiments at modest water content and low stress, *Geology*, *32*(12), 1045-1048.

Karato, S. (2007), *Deformation of Earth Materials: Introduction to the Rheology of the Solid Earth, Cambridge Univ. Press,* New York.

Karato, S., and P. Li (1992), Diffusion creep in perovskite - implications for the rheology of the lower mantle, *Science*, *255*(5049), 1238-1240.

Karato, S. I., M. S. Paterson, and J. D. Fitz Gerald (1986), Rheology of synthetic olivine aggregates - influence of grain-size and water, *J. Geophys. Res.-Solid Earth and Planets*, *91*(B8), 8151-8176.

King, S.D., Lee, C.Y., van Keken, P.E., Leng, W., Zhong, S.J., Tan, E., Tosi, N., Kameyama, M.C., (2010), A community benchmark for 2-D Cartesian compressible convection in the Earth's mantle, *Geophys. J. Int.*, *179*(1), 1-11.

OzBench, M., et al. (2008), A model comparison study of large-scale mantle-lithosphere dynamics driven by subduction, *Phys. Earth Planet. Inter.*, *171*(1-4), 224-234.

Ranalli, G. (2001), Mantle rheology: radial and lateral viscosity variations inferred from microphysical creep laws, *J. Geodyn.*, *32*(4-5), 425-444

Roberts, J. H., and S. J. Zhong (2006), Degree-1 convection in the Martian mantle and the origin of the hemispheric dichotomy, *J. Geophys. Res.-Planets*, *111*, E06013, doi:10.1029/2005JE002668.

Schmeling, H., et al. (2008), A benchmark comparison of spontaneous subduction models towards a free surface, *Phys. Earth Planet. Inter.*, *171*(1-4), 198-223.

Sizova, E., T. Gerya, M. Brown, and L. L. Perchuk (2010), Subduction styles in the Precambrian: Insight from numerical experiments, *Lithos*, *116*(3-4), 209-229.

Stevenson, D. J., and J. S. Turner (1977), Angle of Subduction, *Nature*, *270*(5635), 334-336.

Tackley, P. J. (2000), Mantle convection and plate tectonics: Toward an integrated physical and chemical theory, *Science*, *288*(5473), 2002-2007.

Tan, E., E. Choi, P. Thoutireddy, M. Gurnis, and M. Aivazis (2006), GeoFramework: Coupling multiple models of mantle convection within a computational framework, *Geochem. Geophys. Geosyst.*, *7*, Q06001, doi:10.1029/2005GC001155.

Tovish, A., and G. Schubert (1978), Island arc curvature, velocity of convergence and angle of subduction, *Geophys. Res. Lett.*, *5*(5), 329-332.

Turcotte, D. L., and E. R. Oxburgh (1967), Finite amplitude convection cells and continental drift, J. Fluid Mech., 28, 29-42.

Turcotte, D. L., and G. Schubert (2002), Geodynamics ,Wiley, New York.

van Keken, P. E., and C. J. Ballentine (1999), Dynamical models of mantle volatile evolution and the role of phase transitions and temperature-dependent rheology, *J. Geophys. Res.-Solid Earth*, *104*(B4), 7137-7151.

van Keken, P. E., B. Kiefer, and S. M. Peacock (2002), High-resolution models of subduction zones: Implications for mineral dehydration reactions and the transport of water into the deep mantle, *Geochem. Geophys. Geosyst.*, *3*(10), 1056, doi:10.1029/2001GC000256.

Weertman, J., and J. R. Weertman (1975), High-temperature creep of rock and mantle viscosity, *Annu. Rev. Earth Planet. Sci., 3,* 293-315.

Zhong, S. J., M. T. Zuber, L. Moresi, and M. Gurnis (2000), Role of temperature-dependent viscosity and surface plates in spherical shell models of mantle convection, *J. Geophys. Res.-Solid Earth*, *105*(B5), 11063-11082.

Zhong, S. J., A. McNamara, E. Tan, L. Moresi, and M. Gurnis (2008), A benchmark study on mantle convection in a 3-D spherical shell using CitcomS, *Geochem. Geophys. Geosyst., 9, Q10017,* doi:10.1029/2008GC002048

Figure 2.1. Grid Spacing

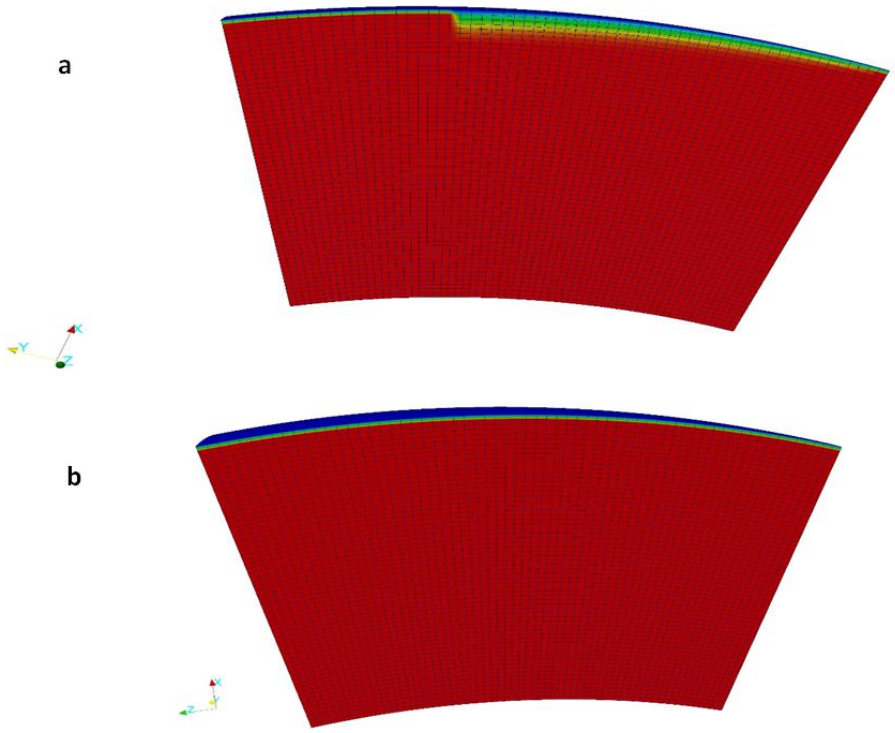

The grid spacing in the model domain a) view of the model along longitude b) view of the model along colatitudes.

Figure 2.2. Model Setup to Show Initial Thermal Profile with Low Viscosity Surface

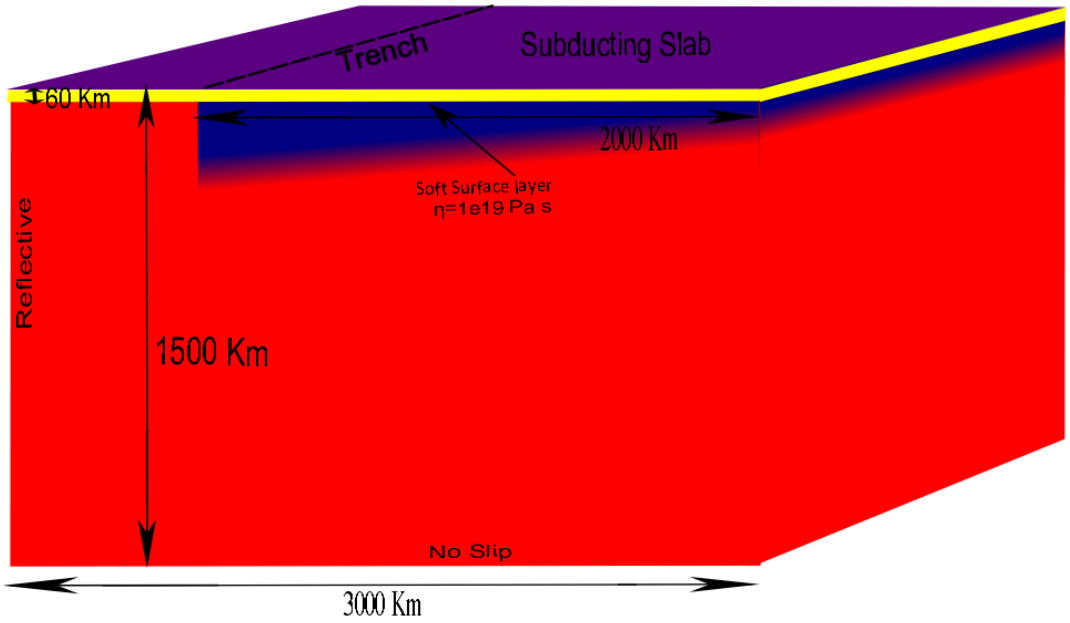

Model setup to show initial thermal profile with low viscosity surface

Figure 2.3. Relative Position of Pole of Rotation on the Earth

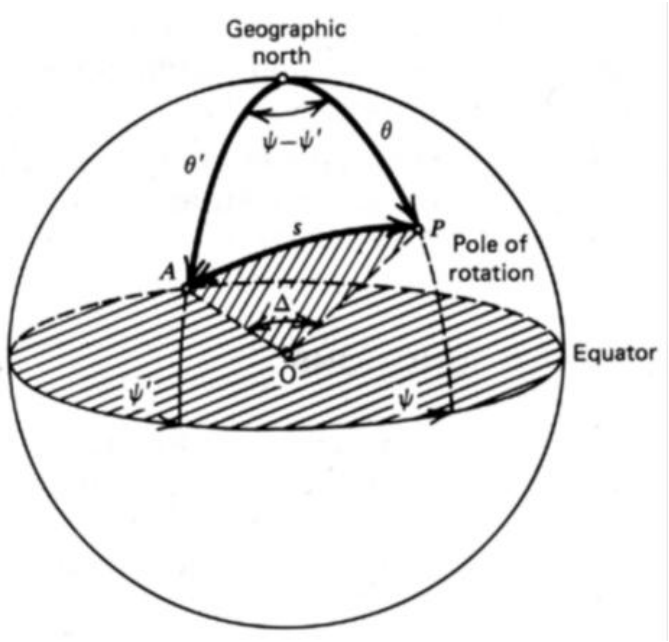

Diagram from Turcotte, D. L., and G. Schubert (2002), Geodynamics ,Wiley, New York. to show the relative position of pole of rotation and a point on the plate boundary. (Used under fair use guidelines, 2012).

Figure 2.4. Imposed Velocity Conditions

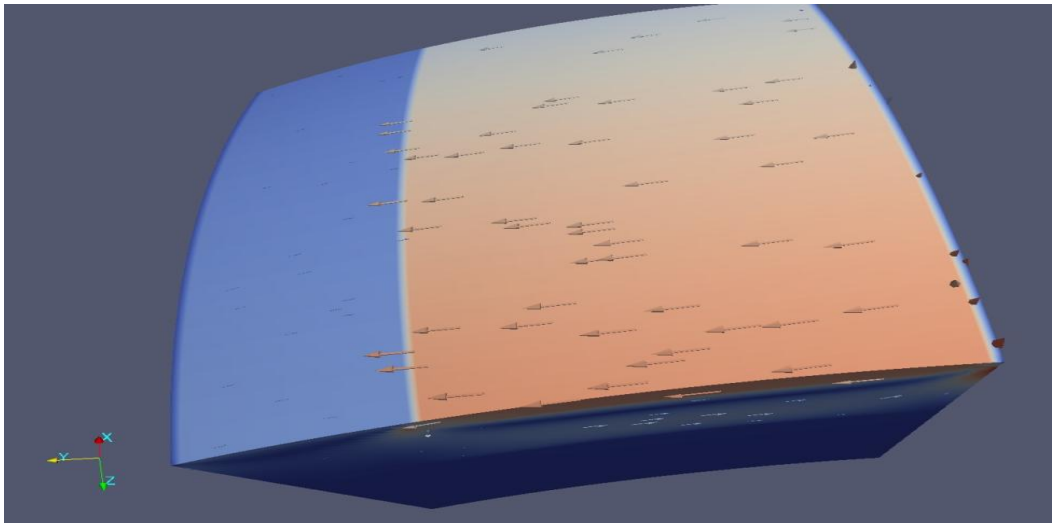

The initial imposed velocity conditions for the model domain. The higher velocity of 5cm/yr is for the slab moving towards the overriding region. The velocity of the overriding region is 2cm/yr.

Figure 2.5. Trench Migration Velocity Conditions

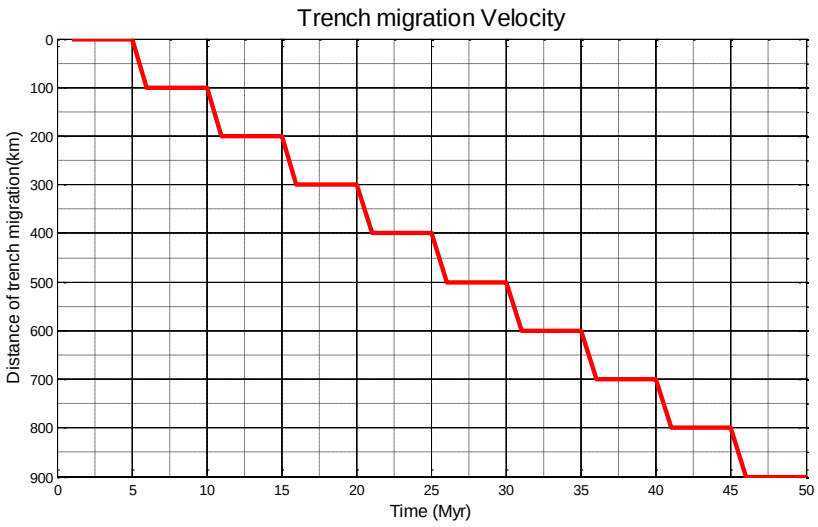

The imposed trench migration velocity conditions for the model domain.

Figure 2.6. Shear Flow Model and LPO Directions

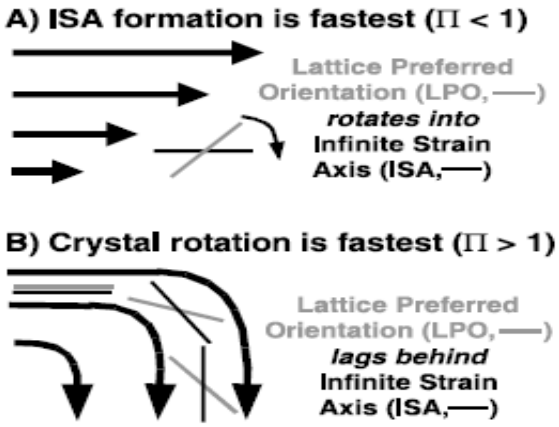

Diagram from Conrad, C. P., M. D. Behn, and P. G. Silver (2007), Global mantle flow and the development of seismic anisotropy: Differences between the oceanic and continental upper mantle, *J. Geophys. Res.-Solid Earth, 112*, B07317, doi:10.1029/2006JB004608. a) Simple shear flow the LPO orientates towards ISA b) Complex flow where the crystal rotation occurs faster than the ISA rotation. The LPO lags behind ISA. (Used under fair use guidelines, 2012).

CHAPTER 3: RESULTS

In this section I first discuss the results that are obtained using a weak "sticky-air layer." The sticky-air layer (Schmeling et al., 2008) provided the entrainment of material and lubrication on the upper part of the slab. Without the sticky air layer I was unable to produce self-consistent subducting slabs. I considered models with plate ages of of 40 Myr, 80 Myr and 120 Myr and varied the Rayleigh number in order to find the range of parameters that allow for realistic subduction. Next I will discuss a set of results with applied trench migration boundary conditions to create the effect of one-sided subduction. Finally the Infinite Strain Axis orientation for the self-consistent stationary trench models with plate ages of 40 Myr, 80 Myr and 120 Myr and the trench-migration model will be discussed.

3.1 Self-consistent Stationary Trench Model

The models are run with a grid of 65x65x65 elements in a spherical shell cap (see Chapter 2 for details). I begin by varying the Rayleigh number in order to identify the parameter regime where the slab sinks through the upper mantle in approximately ~15 Myr, giving a sinking rate for the slab of 660 km/15 Myr = 4.4 cm/yr. I consider three different plate ages, 40 Myr, 80 Myr and 120 Myr and a mechanical thickness of 150 km (i.e., imposed viscosity increase of a factor of 30). Figure 3.1 shows the typical behavior of the depth of the slab tip at different time spans in one of the subduction models with a plate age of 80 Myr. The graph shows how the depth of the tip of the subduction slab varies over time. In the case shown, the slab tip reaches a depth of ~700 km in 15 Myr. This calculation has a Rayleigh number of 10^5. The snapshots at times 5 Myr, 10 Myr and

15 Myr after the initiation of subduction are also shown. I prescribe a plate velocity of 5 cm/yr for 5 Myr to generate an initial negatively buoyant slab, then remove the imposed plate velocity and allow the slab to subduct by itself following the approach of Lee and King (2009).

Figure 3.2 and Figure 3.3 compare the temporal behavior of models with different plate age and different Rayleigh numbers. The plots show the depth of the tip of the slab as function of time as illustrated in Figure 3.1. It should be noted that the time scale starts from 5 Myr rather than 0 Myr because the models are run with an imposed plate velocity for the first 5 Myr as described above. At a Rayleigh number of 10^7 the slab sinks through the transition zone in less than 0.1 Myr, which is geologically unreasonable. For all the plots it should be noted that the older plate (120 Myr) subducts at least by 1 million years sooner than the younger plate (40 Myr) to reach a depth of 670 km because the older plate is more negatively buoyant than the younger plate. Figure 3.4 is the topographic profile of the self-consistent subduction model with an age of 80 Myr plotted using tracers. Between 5-15 Myr the slab subducts by its own but never detaches from the sticky air layer and starts sinking into the mantle. The viscosity of the sticky air layer is about 1000 times less than the viscosity of the slab. But even with low viscosity the subducting plate remains coupled to the slab. Because the sticky air layer and the slab never detaches hence trench rollback is not prominent. It is also noted that the age differences in slab don't alter the velocity pattern conditions the geometry of the subduction only the rate of slab convergence velocity is different. Because the rheology used is non- linear the effective viscosity around the slab is reduced and hence it can subduct easily in the mantle and also supports in the migration of the slab. A very

prominat viscosity jump between the upper and lower mantle is observed as the defromation mechanism in the upper mantle is predominnatly dislocation creep that reduces the effective viscosity whereas the lower mantle is difussion creep.

At an early stage of subduction, about 5 Myr, the subducting slab goes into the mantle with a small change in dip ~20˚ and finally the slab subducts vertically. In subduction model the upper cold dense lithosphere sits over an underlying lighter mantle and is gravitationally unstable. This instability is called the Rayleigh-Taylor instability. Due to this instability, distortion occurs at the fluid interface and the displacement follows as a hyperbolic function. The shape of the displacement looks like diapir. In this model the temperature profile of the vertical part of the subducting slab looks like diapir which is also expected.

3.1.1. Flow Condition

Figures 3.5 through 3.7 are snapshots of calculations at 5, 10 and 15 Myr for initial plate ages of 40 Myr (Figure 3.5), 80 Myr (Figure 3.6) and 120 Myr (Figure 3.7). The three different snapshots in time are shown along different axis orientation to allow the reader to see the three dimensionality of the problem. The first column in Figures 3.5 through 3.7 shows the orientation of the slab along the phi-axis (longitude), the other two orientations are along r-axis (depth). The 2nd column is perpendicular to the vertical is taken at a depth of 440 km and the 3rd column in 660 km. The velocity values vary from 0 cm/yr to 6 cm/yr. It is observed for all the models the flow is above the slab in the mantle wedge region as well as at the back of the slab. The flow in the mantle wedge can be compared with the classic 2D corner flow as shown in Figure 1.4 (see Chapter 1).

However the component of flow parallel to and going around the slab (3D flow) predicted by Long and Silver (2008) is not observed. The flow beneath the slab is much slower than compared to the flow above the slab for all the plate models with different plate ages. From the flow observed in the trench region (2^{nd} and 3^{rd} column) in all the models there is comparatively little or no flow parallel to the trench.

It can be confirmed from the Figures (3.5, 3.6 and 3.7, 1^{st} column) and at a later age that there is a strong corner flow at the back arc of the slab. It is observed that the models with plate age 40 Myr, 80 Myr and 120 Myr the convergence rate of the subducting slab increases with time. Near about 15 Myr the subduction rate of the slab is equal to the initial imposed plate velocity of ~6 cm/yr. At the back-arc of the slab (Figure 3.6, 3.7 and 3.8, column 1^{st}), presence of velocity direction perpendicular to the trench direction is noticed in the range of 2 cm/yr. This type of flow is induced by a viscous shear traction force which occurs due to shear-induced flow from the slab and plate motion and also the viscous drag underneath the plate (Stegman et al., 2006). Since no 3D flow i.e. no trench-parallel flow is observed, no decrease in volume around the slab is present.

3.2 Models with Trench-migration Condition

One of the aim for the study was to see if the introduction of the low viscosity sticky-air layer at the top of the subduction model causes detachment of the slab and hence rollback of the trench. Because the phenomenon of rollback was not observed a new model was developed by imposing a migrating trench using surface velocity boundary conditions that change with time. Figure 3.10 shows the different stages of a

model where the trench migration velocity is imposed by using imposed surface velocity boundary conditions that change with time. The initial age of the plate is 80 Myr and after every 5 Myr the trench is moved toward the ridge a distance of 100 km. It is observed that there is piling of materials and the subduction is also slow indicating that the slab is not negatively buoyant enough to be consistent with the velocity boundary conditions. In this model the viscosity is only temperature dependent. The trench retreats back due to the imposition of trench migration though the use of imposed plate velocities boundary conditions, it should be noted that 3D trench parallel flow is expected around the slab. 3D flow around the slab is noted in the cross-section along r-axis at a depth of 660 km for the time snap shots of 15 Myr, 25 Myr, 35 Myr and 50 Myr.

3.3 Correlation with Grain Orientation Lag Parameter

To quantify whether a certain mantle rheology and slab shape is consistent with observation, I calculate infinite strain axes (ISA) from the predicted mantle flow field (Jadamec and Billen, 2010). The predicted ISA directions can be correlated with SKS fast axis direction (see chapter 1 for details). Following the ISA orientation results from stationary trench and migrating trench, I will try to justify whether seismic anisotropy is sufficient enough to diagnostic the flow field in a subduction zone environment.

3.3.1 Grain Orientation Lag Parameter for Self-consistent Model

Grain orientation Lag (GOL) is a parameter that defines the change of the infinite strain axis orientation along a pathline. An estimation of GOL < 1.0 can be correlated with Infinite Strain Axis (see chapter 2). To investigate the Π value or the Grain Orientation Lag in the subduction region the cross section are taken along the same

orientation as the flow. As with Figures 3.5 through 3.7, the first column shows the orientation of the slab along the phi-axis, the other two orientations are along r-axis. The r-axis defines the depth of the model. The 2nd column is along the r and are taken at a depth of 440 km and the 3rd column in 660 km. It is observed that most of the upper mantle region has an exponential value of -0.5, which corresponds to a Grain Orientation Lag value of 0.3 which means that the rate is ISA orientation is faster that rate of flow and hence ISA orientation will show the approximate LPO direction. In some regions, especially in the region of the overriding plate and at a depth of 660 km the GOL value is greater than 1. In accordance with Conrad et al. (2007) large GOL value are observed in the lower mantle because the large viscosity (30 times more than upper mantle) results in a small strain rate and consequently higher value of Π considering Ω_{flow} constant (see Chapter 2). However, with time the higher value of GOL decreases i.e. it changes to a Π value of 0.8 because of higher strain rate as the subducting slab moves towards the lower mantle. The infinite strain axis orientations in those regions of high GOL cannot be correlated properly. The slow development of ISA in the lower mantle is a hindrance to the stable development of lattice preferred orientation. It is observed that low GOL value is observed in the subducting slab for plate age 80 Myr (Figure 3.9) and 120 Myr (Figure 3.10) near the trench region at a later time of ~15 Myr. This might occur if the vertical component of the density-driven flow spread or converge laterally when it interacts with a rigid boundary (Conrad et al., 2007). At the edge of the model domain there is a high stress because of boundary conditions so the Π value is low.

3.3.2 Grain Orientation Lag Parameter for Trench Migration Model

Figure 3.12 depicts the Π value for a model that has an imposed trench migration velocity. The average Π value for the upper mantle region is a logarithmic value of -0.5 which corresponds to a GOL value of 0.3. At the trench the grain orientation lag is higher than the surrounding. Also it is observed that there is almost no infinite strain axis orientation at the trench. Near the boundary of the model the GOL value is higher close to 1.0. The average Π value for the lower mantle at depth of 660 km is close to a logarithmic 0.8. Plate driven flow induces uniform shear flow and more evenly distributed grain orientation lag value in the upper mantle (Conrad and Behn, 2010). But the GOL value is not uniform as expected. However it should be noted that depth section considered are at 440 km and 660 km far below than the asthenospheric thickness as seen by Conrad et al. (2007) so the result cannot be correlated low GOL value of 10^{-5} is observed which is located between a length 30% to 50% of distance from the trench region. The GOL value is quite low at the edge of the model domain this is because of high strain associated due to discontinuity in the model and other plate boundary conditions. In accordance with the imposed velocity and layered viscosity model of Conrad et al. (2007), the depth section (at a depth of ~440 km) Figure (3.12 a, b, c and d 1st column) faint orange tinge in the middle corresponding to a Π value of 1.0 is seen that corresponds to the white patch seen by Conrad et al. (2007) for their model. However Conrad et al. (2007) saw that the GOL value for the lithosphere is higher than the asthenosphere which is not observed in this trench-migration model.

3.4 Correlation with Infinite Strain Axis

3.4.1 Correlation with Infinite Strain Axis for Self-consistent Model

The Grain Orientation Lag values for the self-consistent models (Figure 3.8, 3.9, 3.10) are less than 1, which means that most of the models, the ISA orientations will be a good approximation to the LPO direction. Jadamec and Billen (2010) showed that composite viscosity closely follow ISA directions hence the ISA self-consistent stationary trench models will be more closely correlated. ISA direction is most sensitive to shear stress (Conrad et al., 2007). Because in all these self-consistent stationary trench models up to a time of 5 Myr the subduction occurs by plate driven velocities, infinite strain axis direction orientates itself to the shear directions After 5 Myr the flow is mostly driven by viscous flow as the slab is allowed to subduct self-consistently. Because of density differences and zones of weakness the slab subducts self-consistently. The strain rate for density driven component is inversely proportional to absolute viscosity (Behn et al., 2004). The viscosity is lower at the depth of 440 km than 660 km this will makes strain rate higher at the shallower depth of 440 km. The overall GOL value is higher at the depth of 660 km compared to depth of 440 km. The ISA directions calculated after 5 Myr are parallel to the shear direction or the plate velocity direction. For the later times i.e. at 10 Myr and 15 Myr the ISA directions are in accordance to the mantle flow direction. For all the models with plate age of 40 Myr, 80 Myr and 120 Myr it is observed that in the trench region (2^{nd} and 3^{rd} column) ISA is in the direction of flow and consequently the LPO direction is trench perpendicular. Near region of vertical flow (i.e. at the trench region) there is less to no ISA development. In these self–consistent

subduction models with stationary trench (Figures 3.8, 3.9 and 3.10) it is observed that flow as well as ISA orientation is trench perpendicular. No ISA orientation is observed at the trench region because of the vertical flow dominates the horizontal flow. At a depth of 660 km especially for the model with age 80 Myr (Figure 3.9c) some non-trench parallel ISA orientations are also observed the reason for this is not very well explained but since vertical flow dominates over the horizontal flow or it might be a component of the vertical ISA orientation. It is also noted that at the region (column 1) where the vertical flow is maximum no ISA orientation is observed. But the orientation of the ISA aligns with the corner flow direction.

3.4.2 Correlation with Infinite Strain Axis for Trench Migration Model

The infinite strain axis directions can be correlated with the Π value wherever it is less than 1. ISA direction is most sensitive to shear deformation and orients to the direction of maximum shear in case of plate driven motion (Conrad et al., 2007). In the trench migration model the subduction is caused by imposed plate velocity conditions and imposed trench migration velocity. As pointed out by Conrad et al. (2007), the ISA is parallel to the maximum shear stress in plate driven flow so comparing Figure 3.11 (column 2 and column 3) and Figure 3.12 (column 2 and column 3) it can be correlated that ISA is in the flow direction. It is also observed that ISA direction is mostly trench perpendicular beneath the subducting slab. In Figure 3.12 (a, b, c and d column 3rd) some orientation of the ISA is observed which not trench parallel is but is at an angle to the trench. It should also be noted that there is no flow in that part of model. The mantle is more or less stationary. Such ISA directions occur because of change in the stress

conditions. However, if the mantle is driven by viscous flow then anisotropic prediction of GOL value less than 0.5 is ignored (Conrad et al., 2007). Near the overriding plate region no ISA orientation is observed at a depth of 660 km but some ISA orientation is still observed at the depth of 440 km this could be because of the fact that shear flow is more prominent in the upper part of the subduction region. The trench perpendicular behavior is also observed may be because of the fact the rate of trench-migration is less than the convergence velocity and hence anisotropy is more trench-perpendicular (refer to Figure 1.3).

3.5 Discussion

The sensitivity of seismic anisotropy to flow characteristics in the subduction region is important to quantify and to see if this can be used as tool to identify flow in the subduction region from observed anisotropy. In this study both model with stationary trench and migrating trench are formulated as the infinite strain axis directions predicted from these models are correlated to comment on flow. As is observed from Figure 3.6 and Figure 3.11 for a plate age of 80 Myr it can be inferred that the flow direction is clearly very different in both the cases. From Figure 3.9 it can be inferred that there is presence of corner flow in the subduction region, but the trench migration model (Figure 3.11) shows some presence of 3D flow with no corner flow. By comparing the difference in the grain orientation lag Figure 3.12 (2^{nd} and 3^{rd} column) and Figure 3.9 (2^{nd} and 3^{rd} column), it is observed that in case of a stationary trench, self-consistent model, the GOL distribution is more consistent. However in the case of the trench-migration model, the GOL distribution is not consistent as expected because it is driven by plate motions. There is a region of low GOL value at the center of the model. While comparing the ISA

orientation in the two models the basic trend in the models almost remains the same which is trench perpendicular. The orientation is perpendicular to the trench. The trench-migration model (Figure 3.11, third column) has a 3D flow pattern around the slab but even such a flow pattern does not contribute to any change in the ISA orientation in the two models which is expected to be trench-parallel. The trench non-parallel ISA directions observed at a depth of 660 km could occur due to viscous flow. But if it is considered that the trench non-parallel directions occur because of 3D flow then ISA can be used as a tool to define flow parameter. According to Long and Silver (2008) the shear wave splitting measurements that define LPO directions provide direct constrain to the geometry of the upper mantle deformation and the upper mantle flow. But LPO directions as observed from the ISA orientation in both the stationary trench and migrating trench show mostly a trench-perpendicular orientation even with very different flow pattern except for a bit of trench non-parallel orientation. So it is controversial if LPO directions can be used to constrain flow pattern. It appears that the ISA directions is always pointing to the plate motion direction and doesn't change even when the plate is allowed to subduct by its own (Figure 3.9, column 2^{nd} and 3^{rd}).

The basic parameter that was neglected in the self-consistent model was the resolution of the sticky-air layer. The grid size was bigger compared to the thickness of the sticky-air layer. I also neglected the effect of the lateral viscosity contrast possible due to asthenospheric channels. In this model a low viscosity sticky air layer is used which is an assumption of a free surface. Following the second approach of Schmelling et al. (2008) a free-surface condition need to be imposed. However, during the course of the research the model parameter was used but there were some problem in imposing the

free-surface. The model with trench-migration velocity subducts very slowly. This implies that in comparison to simple temperature-dependent viscosity it requires weakening of the slab due to power law rheology or yield stress or due to presence of low viscosity fault region. Parmentier and Morgan (1982) showed that there is a correlation between boundary layer scaling that predicts a temperature difference which is proportional to $Ra^{-1/5}$ at large Ra. They also figured out that there is a relation of Rayleigh number to Nusselt number and depending on the boundary condition such as the no-slip or stress-free boundary condition. They saw those different proportionality exponents are used for different boundary conditions. This might be a method which needs to be considered when working with high Rayleigh number.

The model with trench-migration velocity subducts very slowly. This implies that in comparison to simple temperature-dependent viscosity it requires weakening of the slab due to power law rheology or yield stress or due to presence of low viscosity fault region. The viscosity of the subducting slab at the trench region is important to control the slab dynamics. Large bending stresses are required for slab weakening in the trench region. Slab weakening in the trench region can accelerate the subduction.

References

Billen, M. I., and G. Hirth (2007), Rheologic controls on slab dynamics, *Geochem. Geophys Geosyst., 8*, Q08012, doi:10.1029/2007GC001597

Behn, M. D., C. P. Conrad, and P. G. Silver (2004), Detection of upper mantle flow associated with the African superplume, Earth Planet. Sci. Lett., 224, 259 – 274, doi:10.1016/j.epsl.2004.05.026

Conrad, C. P., and M. Gurnis (2003), Seismic tomography, surface uplift, and the breakup of Gondwanaland: Integrating mantle convection backwards in time, *Geochem. Geophys. Geosyst., 4*(3), 1031, doi:10.1029/2001GC000299

Conrad, C. P., and M. D. Behn (2010), Constraints on lithosphere net rotation and asthenospheric viscosity from global mantle flow models and seismic anisotropy, *Geochem. Geophys. Geosyst., 11*, Q05W05, doi:10.1029/2009GC002970

Conrad, C. P., M. D. Behn, and P. G. Silver (2007), Global mantle flow and the development of seismic anisotropy: Differences between the oceanic and continental upper mantle, *J. Geophys. Res.-Solid Earth, 112*, B07317, doi:10.1029/2006JB004608.

Jadamec, M. A., and M. I. Billen (2010), Reconciling surface plate motions with rapid three-dimensional mantle flow around a slab edge, *Nature,*465, 338–341, doi:10.1038/nature09053

Long, M. D., and P. G. Silver (2008), The subduction zone flow field from seismic anisotropy: A global view, *Science*, *319*(5861), 315-318.

Parmentier, E. M., and J. Morgan (1982), Thermal convection in non-Newtonian fluids:

Volumetric heating and boundary layer scaling, *J. Geophys. Res.*, *87*, 7757-7762

Schmeling, H., et al. (2008), A benchmark comparison of spontaneous subduction models towards a free surface, *Phys. Earth Planet. Inter.*, *171*(1-4), 198-223.

Stegman, D. R., J. Freeman, W. P. Schellart, L. Moresi, and D. May (2006), Influence of trench width on subduction hinge retreat rates in 3-D models of slab rollback, *Geochem. Geophys. Geosyst.*, *7*, Q03012, doi:10.1029/2005GC001056

Figure 3.1. Temporal Behavior of Self-consistent Subduction Model

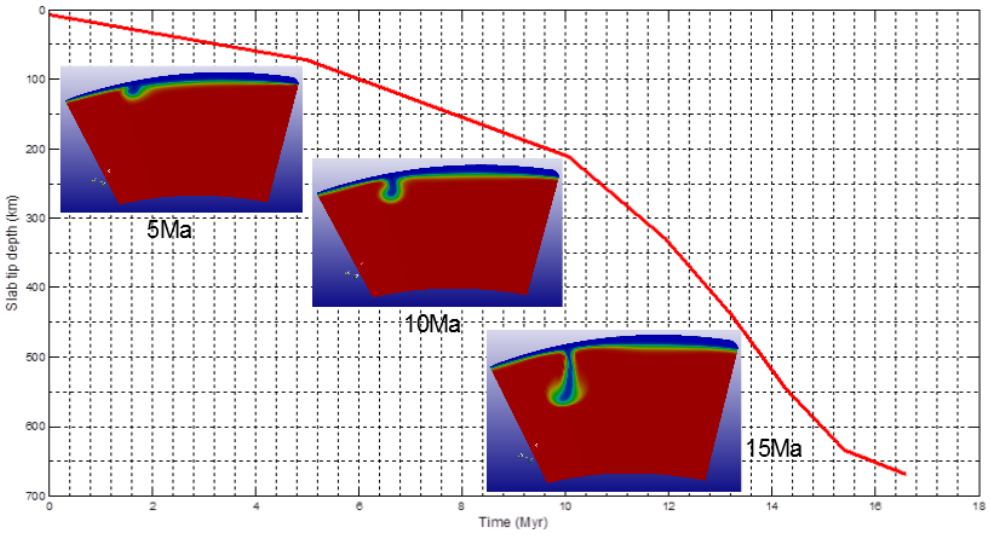

Temporal behavior of self-consistent subduction model with age of 80 Myr. The curve shows the slab tip depth as a function of Time in Myr. Snap shot of subduction is shown at different time of 5Ma, 10Ma and 15Ma respectively .The resolution of the model is 65x65x65.

Figure 3.2. Temporal Behavior of Self-consistent Subduction Model at Different Rayleigh Number

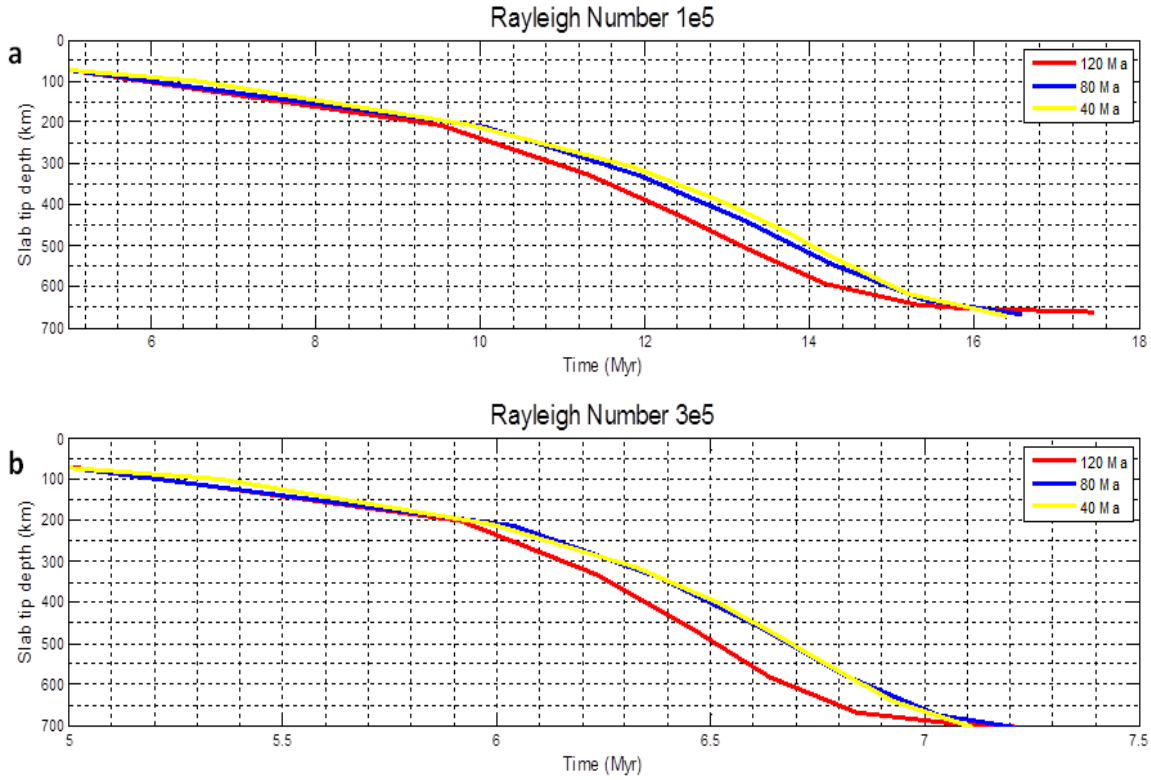

Temporal behavior of self-consistent subduction model at different Rayleigh Number. The legends show the age of the plate. a) Rayleigh Number of 1e5 b) Rayleigh Number of 3e5 .The color index shows the age of plates. The curve shows the slab tip depth as a function of time in Myr.

Figure 3.3. Temporal Behavior of Self-consistent Subduction Model at Different Rayleigh Number

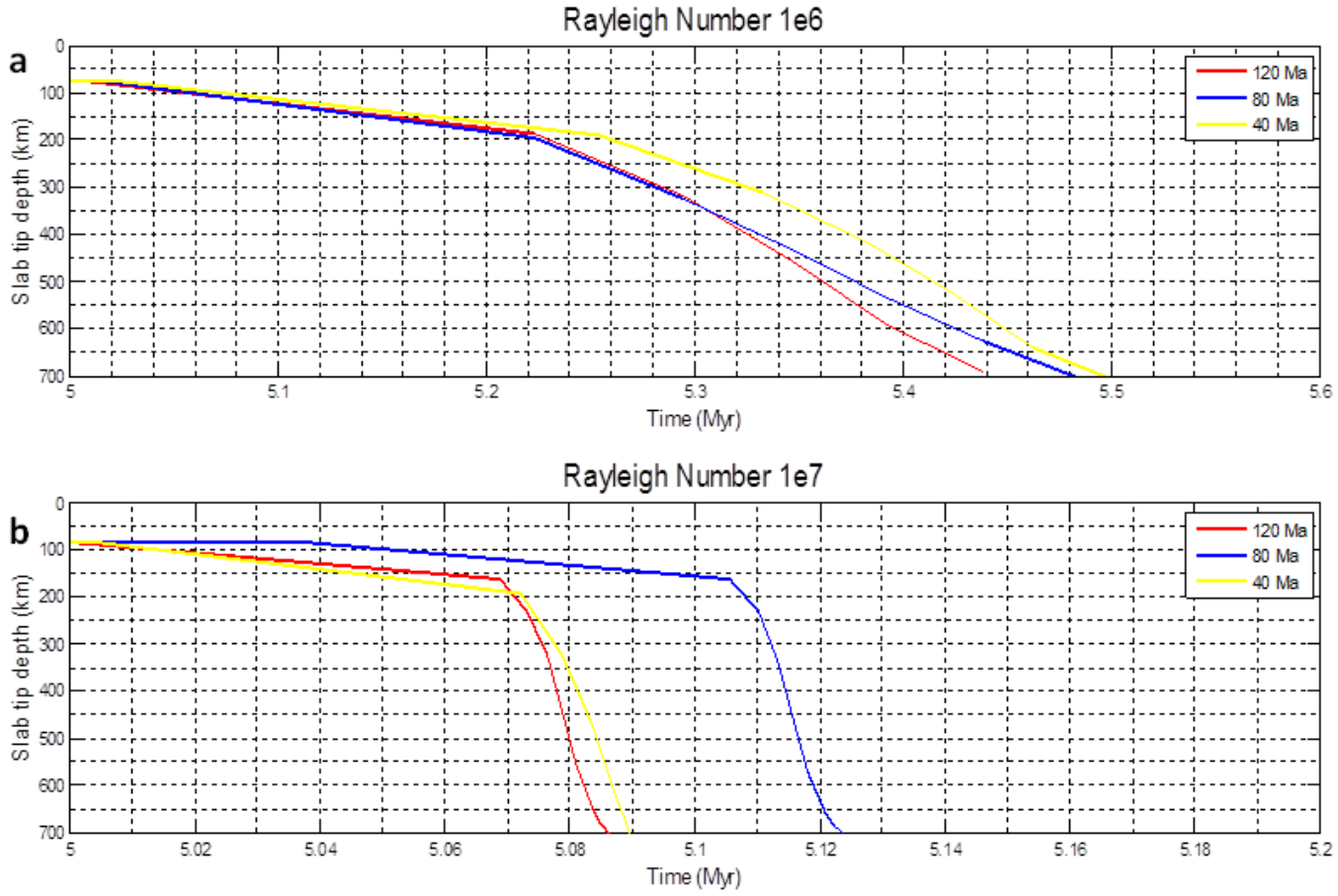

Temporal behavior of self-consistent subduction model at different Rayleigh Number. The legends show the age of the plate. a) Rayleigh Number of 1e6 b) Rayleigh Number of 1e7 .The color index shows the age of plates. The curve shows the slab tip depth as a function of time in Myr.

Figure 3.4. Subduction Profile

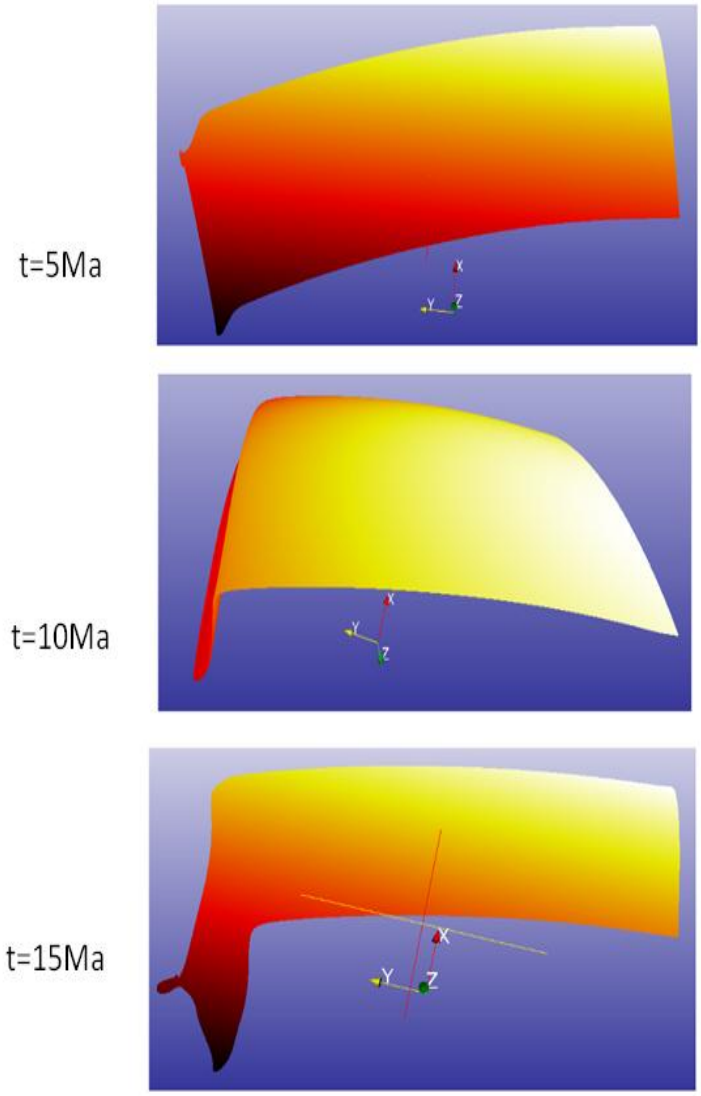

The subduction profile for the Plate with age 80 Myr. The color scheme is not to scale but to show the effect of bending of the slab

Figure 3.5. Slab Evolution for a Plate Age 40 Ma

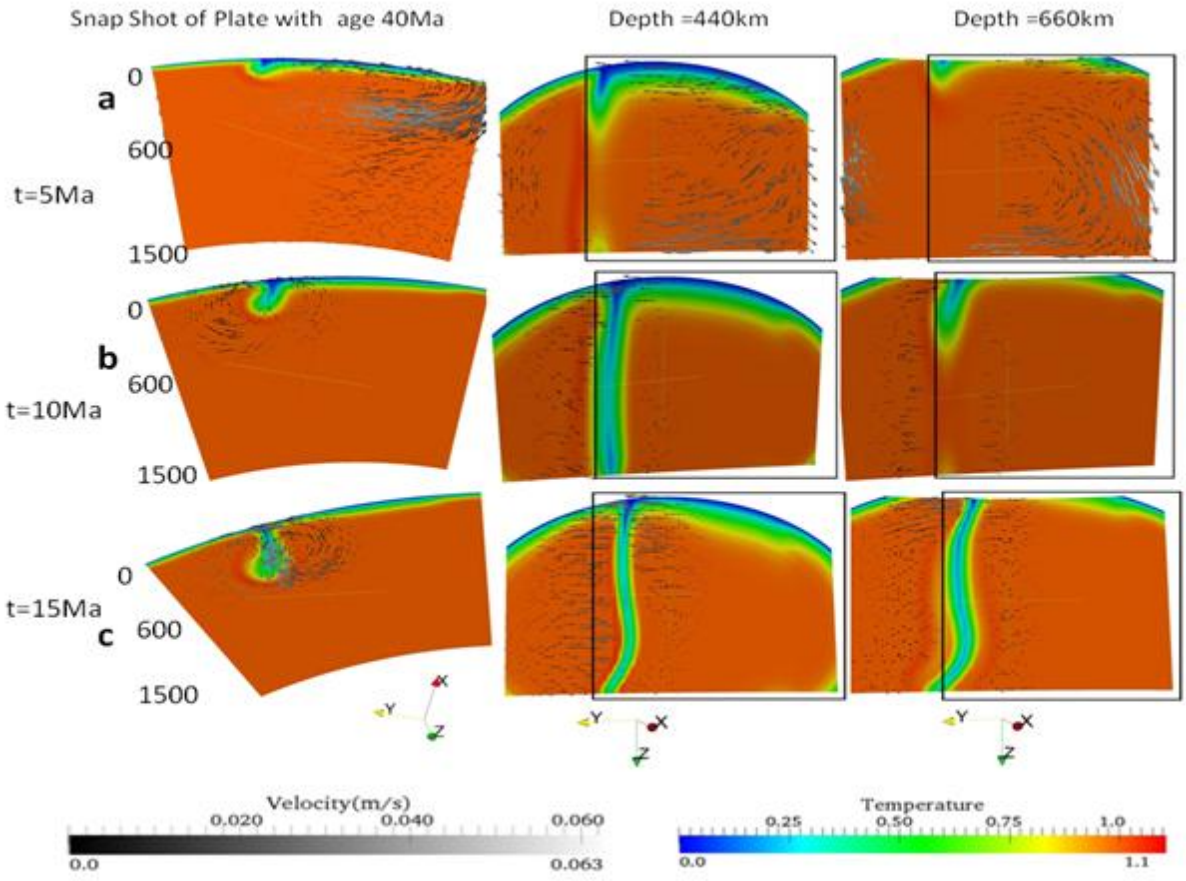

Slab evolution for a young plate age 40 Ma. The first column is representation along phi –axis and the second and third column is representation along r-axis. The two different columns are representation at a depth of 440 km and 660 km respectively. The boxes represent the region of the subducting plate. (a) After a time of 5 Ma (b) After a time of 10 Ma (c) After a time of 15 Ma.

Figure 3.6. Slab Evolution for a Plate Age 80 Ma

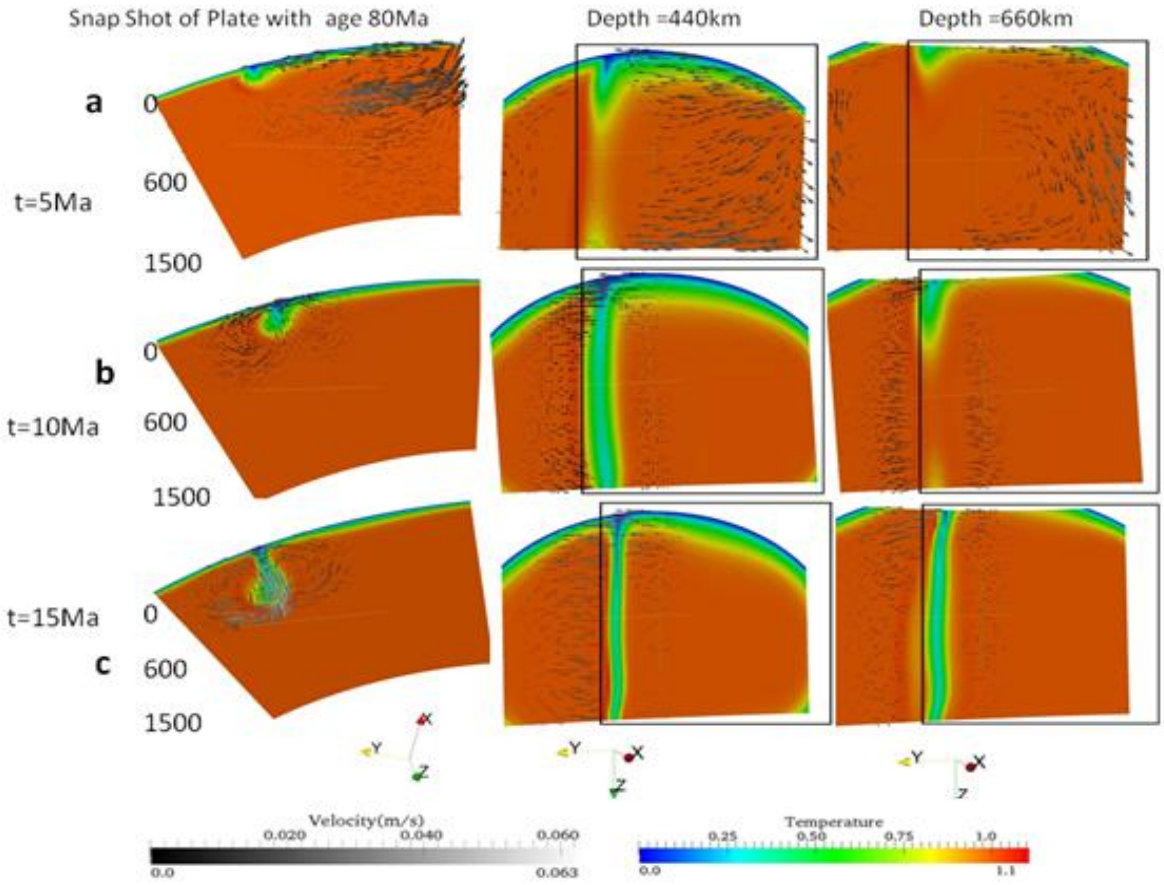

Slab evolution for an intermediate plate age 80Ma. The first column is representation along phi–axis and the second and third column is representation along r-axis. The two different columns are representation at a depth of 440 km and 660 km respectively. The boxes represent the region of the subducting plate. (a) After a time of 5Ma (b) After a time of 10Ma (c) After a time of 15Ma.

Figure 3.7. Slab Evolution for a Plate Age 120 Ma

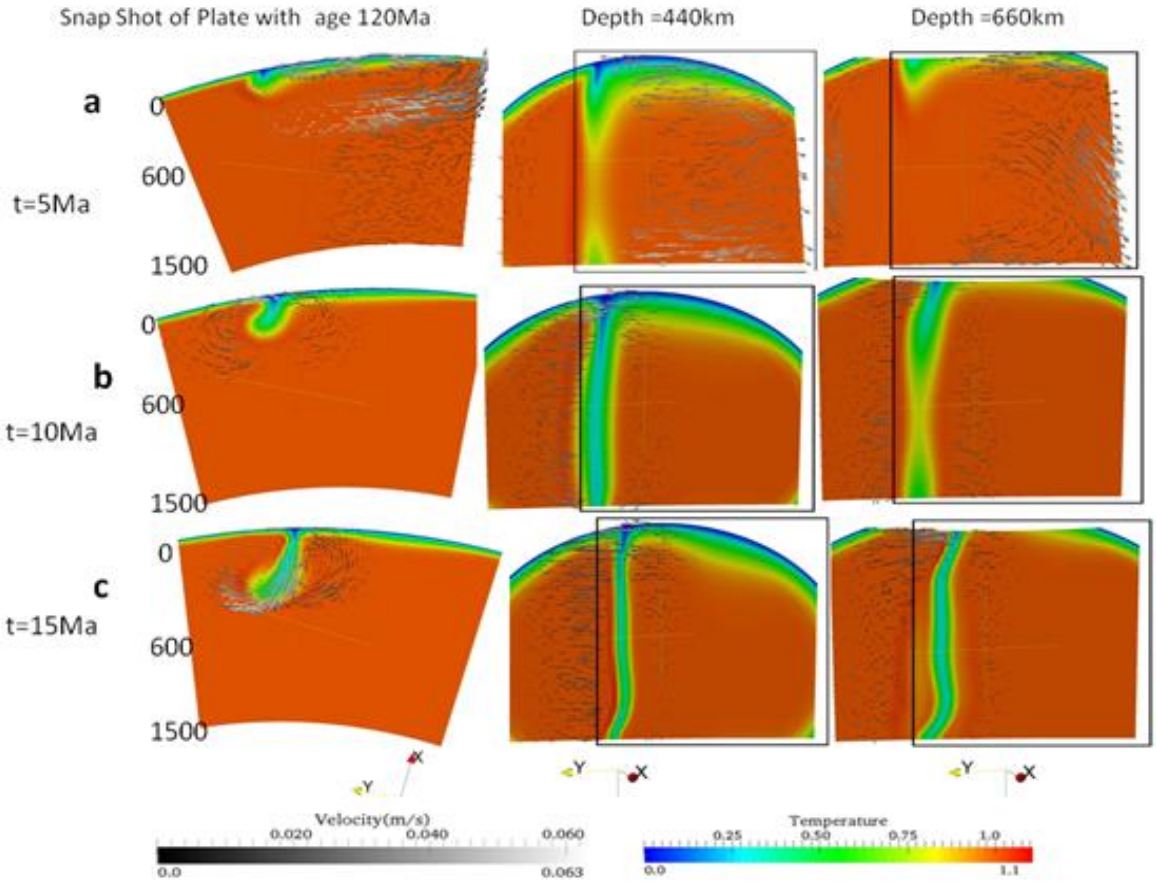

Slab evolution for an older plate age 120Ma. The first column is representation along phi –axis and the second and third column is representation along r-axis. The two different columns are representation at a depth of 440 km and 660 km respectively. The boxes represent the region of the subducting plate. (a) After a time of 5Ma (b) After a time of 10Ma (c) After a time of 15Ma.

Figure 3.8. GOL and ISA Orientation for a Plate Age 40 Ma

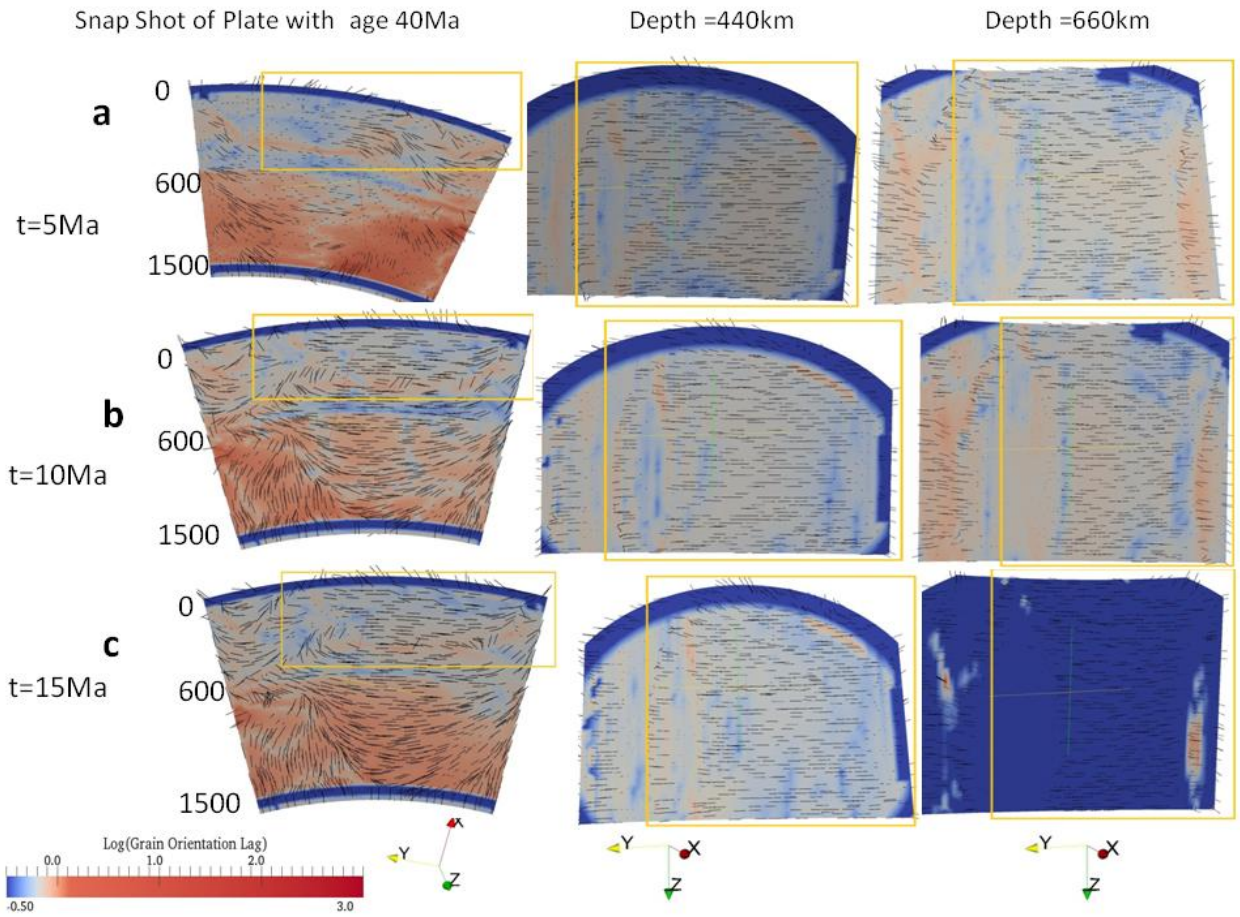

Slab evolution for a younger plate age 40 Ma. The first column is representation along phi–axis and the second and third column is representation along r-axis. The two different columns are representation at a depth of 440 km and 660 km respectively. The boxes represent the region of the subducting plate. (a) After a time of 5 Ma (b) After a time of 10 Ma (c) After a time of 15 Ma.

Figure 3.9. GOL and ISA Orientation for a Plate Age 80 Ma

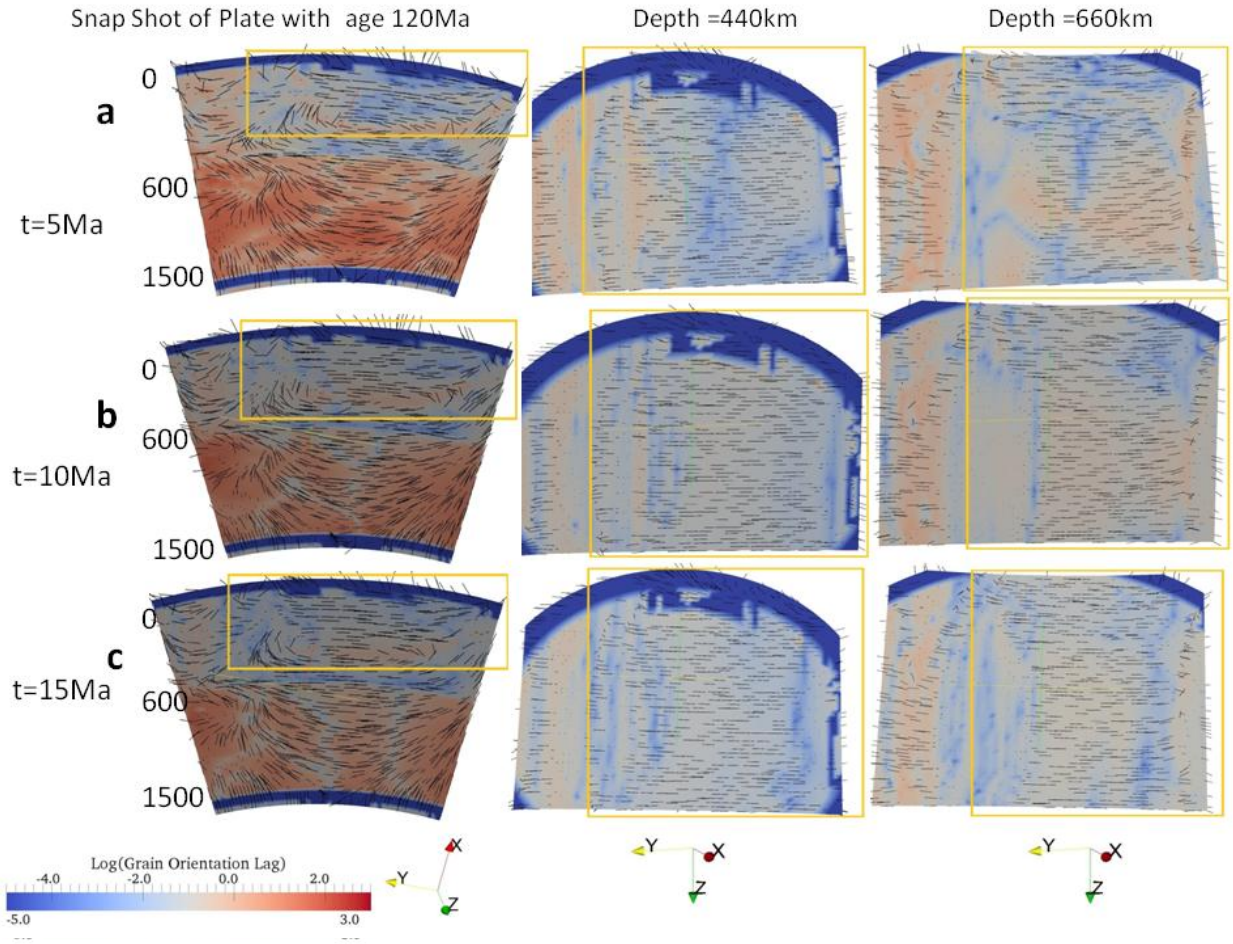

Slab evolution for an intermediate plate age 80 Ma. The first column is representation along phi–axis and the second and third column is representation along r-axis. The two different columns are representation at a depth of 440 km and 660 km respectively. The boxes represent the region of the subducting plate. (a) After a time of 5 Ma (b) After a time of 10 Ma (c) After a time of 15 Ma.

Figure 3.10. GOL and ISA Orientation for a Plate Age 120 Ma

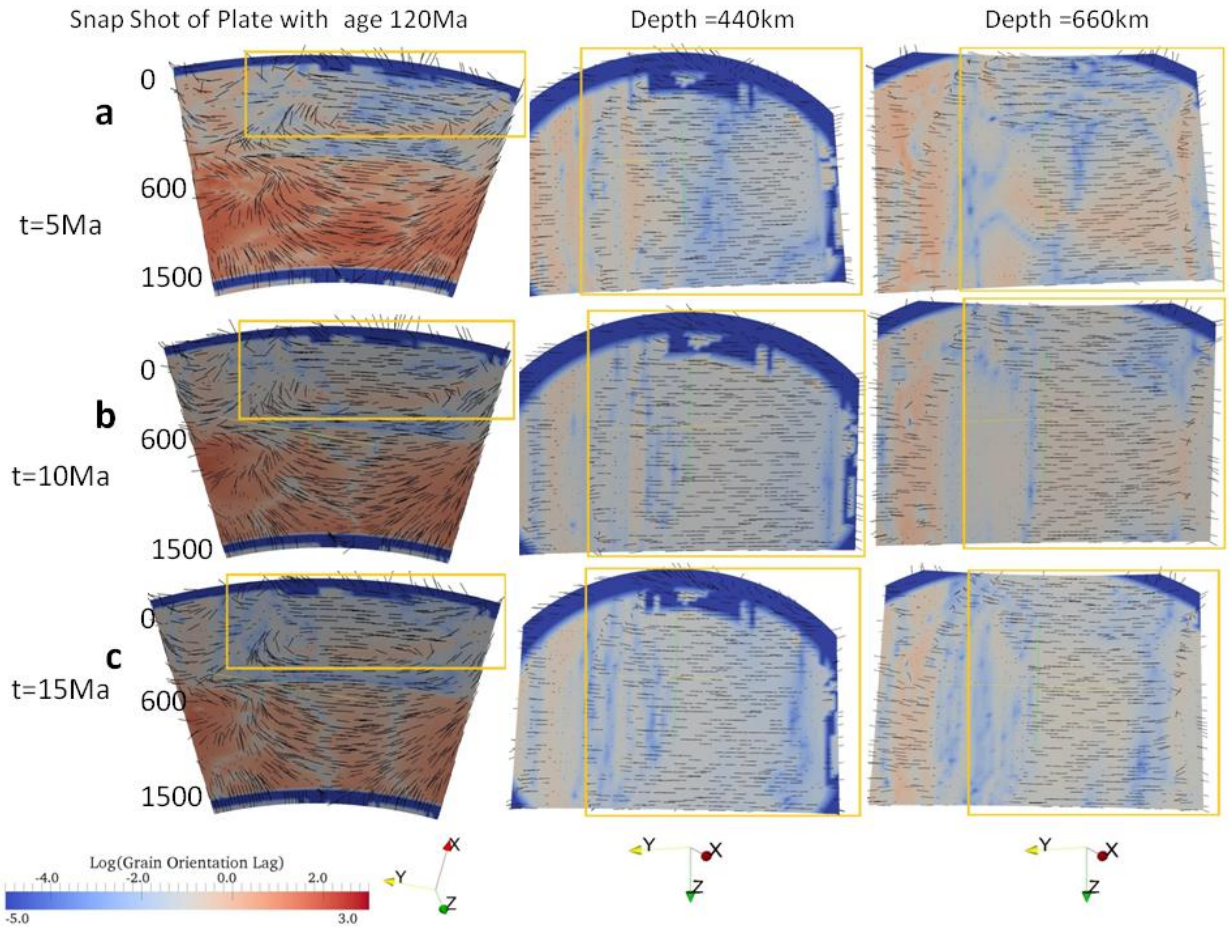

Slab evolution for an older plate age 120 Ma. The first column is representation along phi–axis and the second and third column is representation along r-axis. The two different columns are representation at a depth of 440 km and 660 km respectively. The boxes represent the region of the subducting plate. (a) After a time of 5 Ma (b) After a time of 10 Ma (c) After a time of 15 Ma.

Figure 3.11. Slab Evolution for Trench Migration Model

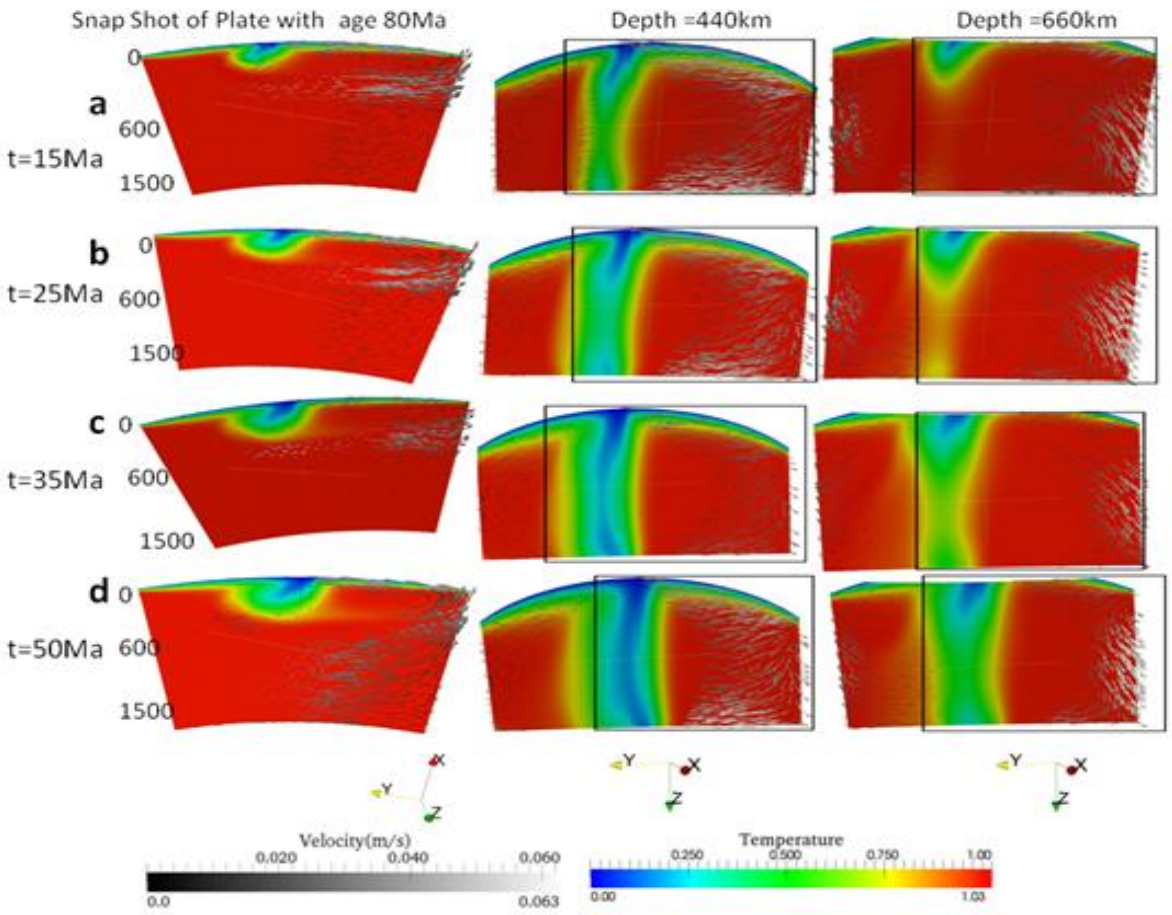

Slab evolution for plate age 80 Ma with applied trench migration. The first column is representation along phi–axis and the second and third column is representation along r-axis. The two different columns are representation at a depth of 440 km and 660 km respectively. The boxes represent the region of the subducting plate. (a) After a time of 15 Ma (b) After a time of 25 Ma (c) After a time of 35 Ma and (d) After a time of 50 Ma.

Figure 3.12. GOL and ISA Orientation for Trench Migration Model

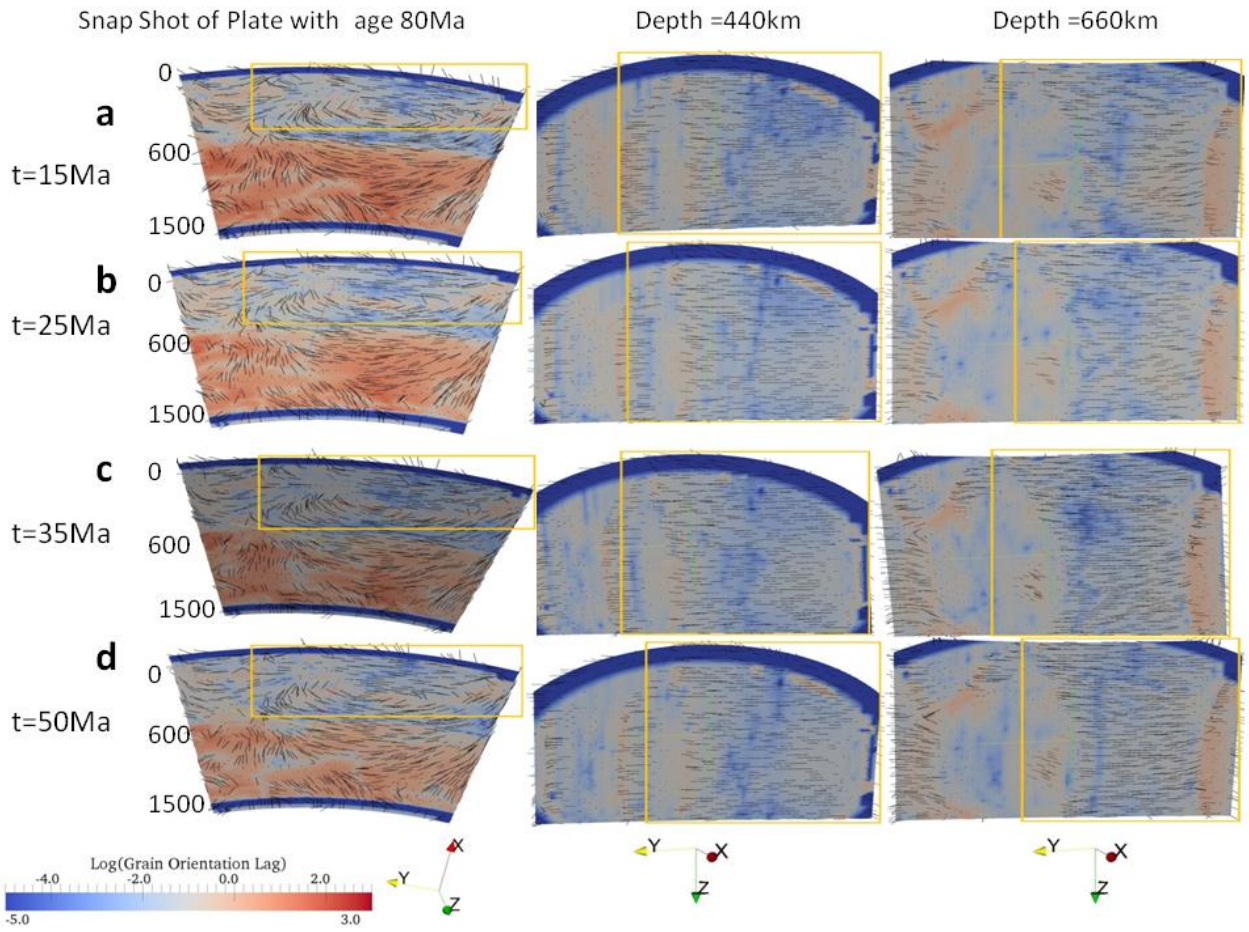

Slab evolution for plate age 80Ma with applied trench migration. The first column is representation along phi–axis and the second and third column is representation along r-axis. The two different columns are representation at a depth of 440 km and 660 km respectively. The boxes represent the region of the subducting plate. (a) After a time of 15Ma (b) After a time of 25Ma (c) After a time of 35Ma and (d) After a time of 50Ma.

CHAPTER 4: CONCLUSION AND FUTURE WORK

At subduction zones on Earth both trench-parallel and trench-perpendicular seismic anisotropy directions are observed. Seismic anisotropy is considered as a proxy for the mantle flow field but, the present study shows that the mantle flow field might not be the only factor that causes LPO orientation. The LPO direction in the mantle wedge from two models the self-consistent stationary trench model and migrating trench model both have trench-perpendicular orientation. According to Long and Silver (2008) predictions, two competing flow fields modify the seismic anisotropy directions. They argued that if the velocity of trench migration is higher than the subduction velocity then 3D flow around the slab is prominent causing trench-parallel anisotropy orientation. Following this statement my model with migrating trench does not show trench-parallel orientations because the convergence velocity is ~3cm/yr compared to the migration velocity of the trench in the range of ~3-4cm/yr and the migration velocity is not too big compared to convergence velocity. My model is not entirely consistent with the Long and Silver (2008) model because the model with migrating trench does not show trench-parallel behavior even though the only mantle flow field observed is 3D flow around the slab, but the model validates the argument the trench-migration velocity should be greater than convergence velocity to see trench-parallel anisotropy. Because the self-consistent stationary trench model show strong 2D corner flow, hence the LPO orientation in the trench-perpendicular direction is valid. However if there is mostly 2D corner flow (e.g. Ryukyu trench), then the temperature condition in the mantle wedge causes B-type olivine. But in the present context no low temperature condition is observed in the mantle

wedge for both stationary and migrating models. However it should be noted that the stationary model is stress-dependent viscosity while the migrating trench is only temperature dependent. Jung and Karato (2001) and Karato et al. (2008) stated that the presence of water can cause significant change in the deformation mechanism of LPO. Laboratory measurements for olivine deformation (Jung and Karato, 2001; Karato et al., 2008 and Hirth and Kohlstedt, 2003) have provided significant change in the LPO direction in presence of water. In order to study whether the mantle flow pattern is the only cause of seismic anisotropy, it is necessary to include a) water conditions (i.e. water fugacity) in the mantle wedge b) regions of coupling and decoupling in the subducting slab (Kneller et al., 2007) c) presence of shear heating in the model.

A limitation of the present model is that the self-consisting subducting slab does not decouple from the top low viscosity sticky-air layer of the model (i.e. layer that mimics the free-surface). Hence the trench rollback phenomenon is not observed in the self-consistent model. The major cause of this problem could be the thickness of "sticky-air" layer. Decoupling of the slab from the "sticky-air" layer might be limited by the parameters used here. Using a finer mesh grid could have averted this problem. Decreasing the viscosity factor of the "sticky-air" might also be important for the decoupling of the slab. The phase changes in the olivine system at 410 km and 660 km are also neglected in this study. Zhong and Gurnis (1995) showed that phase change dynamics causes more epidosity in terms of rollback dynamics. Billen and Hirth (2007) argued that reflecting boundary conditions create a reference frame which is fixed with respect to the model domain. Using reflecting boundary conditions as sidewall boundary condition for the self-consistent model could have restricted the motion of the trench. The

use of periodic boundary conditions (Enns et al., 2005; Stegmann et al., 2006) causes motion of the trench with respect to the mantle. In my self-consistent model the subducting slab rolls forwards near the upper mantle and lower mantle boundary. This result is contradictory to Billen and Hirth (2007) findings with a model domain thickness of 1500 km where the slab rolls backward. This can be attributed to the difference in the upper and lower mantle viscosity ratio.

Chertova et al., (2012) argued that that presence of open sidewalls in a 2D subduction model allows for the lateral in- and outflow mantle consistent with the internal dynamics of the model. Such inflow and outflow of mantle material will be very close to the real-mantle environment of subduction. They also argued that there is always a return flow in mantle that is not observed by the open and closed (free-slip) sidewalls for 2D models. The effect of the 3D model might help to remove some of those limitations but it would be preferable to observe a 3D model where the sidewalls are open. To build on this work one should remove the sidewall boundary such that the subduction model is embedded into a spherical Earth and the sidewall boundary is removed. The plate velocities imposed on the spherical Earth can be imposed from the NUVEL-1A model by DeMets et al. (1994). One of the future applications is to apply the subduction model to real Earth data. One of the examples would be the subduction zone in NE Japan. It has been observed from shear wave polarization waveforms of the intermediate depth Earthquake beneath the Northeast Japan, that there is correlation between delay time and anisotropy direction throughout the mantle wedge (Nakajima and Hasegawa, 2004). If this self-consistent subduction model can be used to test the strength

of the slab; whether the pattern of mantle flow will be around slab (i.e. strong slab) or if the slab is weak enough to rollback.

References

Billen, M. I., and G. Hirth (2007), Rheologic controls on slab dynamics, *Geochem. Geophys Geosyst., 8*, Q08012, doi:10.1029/2007GC001597

Chertova, M., Geenen, T., van den Berg, A., and Spakman, W. (2012): Using open sidewalls for modeling self-consistent lithosphere subduction dynamics, Solid Earth Discuss., 4, 707-744, doi:10.5194/sed-4-707.

Long, M. D. & Silver, P. (2008), The subduction zone flow field from seismic anisotropy: a global view. Science, *319*, 315–318

DeMets, C., R.G. Gordon, D.F. Argus, and S. Stein (1994), Effect of recent revisions to the geomagnetic reversal time scale on estimates of current plate motions, *Geophys. Res. Lett.*, *21*, 2191-2194.

Enns, A., T. W. Becker, and H. Schmeling (2005), The dynamics of subduction and trench migration for viscosity stratification, *Geophys. J. Int.*, *160*(2), 761-775.

Hirth, G., and D. L. Kohlstedt (2003), Rheology of the upper mantle and themantle wedge: A view from the experimentalists, in Inside the Subduction Factory, Geophys. Monogr., vol. 138, edited by J. Eiler, pp. 83–105, AGU, Washington, D. C.

Jung, H. & Karato, S. I. (2001), Water-induced fabric transitions in olivine. Science 293, 1460–1463.

Karato, S., H. Jung, I. Katayama, and P. Skemer (2008), Geodynamic significance of

seismic anisotropy of the upper mantle: New insights from laboratory studies, *Annual Review of Earth and Planetary Sciences*, 59-95.

Kneller, E.A., van Keken P.E., Karato S., J. Park (2005), B-type olivine fabric in the mantle wedge: insights from high-resolution non-Newtonian subduction zone models,*Earth Planet. Sci. Lett.* 237, 781–97

Nakajima, J., and A. Hasegawa (2004), Shear-wave polarization anisotropy and subduction-induced flow in the mantle wedge of northeastern Japan, *Earth Planet. Sci. Lett*., 225, 365-377.

Stegman, D. R., J. Freeman, W. P. Schellart, L. Moresi, and D. May (2006), Influence of trench width on subduction hinge retreat rates in 3-D models of slab rollback, *Geochem.Geophys. Geosyst., 7,* Q03012, doi:10.1029/2005GC001056.

Zhong, S. J., and M. Gurnis (1995), Mantle convection with plates and mobile, faulted plate margins, Science, 267, 838-843